Reverse Phase Protein Array Reveals Correlation of Retinoic Acid Metabolism With Cardiomyopathy in Friedreich's Ataxia

Authors

Jill S. Napierala, Kimal Rajapakshe, Amanda Clark, Yu-Yun Chen, Shixia Huang, Clementina Mesaros, Peining Xu, Ian A. Blair, Lauren A. Hauser, Jennifer Farmer, David R. Lynch, Dean P. Edwards, Cristian Coarfa, and Marek Napierala

Correspondence

jsbutler@uab.edu; mnapiera@uab.edu

In Brief

We conducted a sensitive and high-throughput reverse phase protein array to attain protein expression profiles of primary fibroblasts from patients with Friedreich's ataxia (FRDA) and unaffected controls using a pool of 217 validated antibodies. Our extensive bioinformatics analyses correlated differentially expressed (DE) proteins with critical disease parameters. Expression levels of several integrin proteins specifically associated with hearing loss in FRDA. Also, reverse phase protein array data integrated with transcriptome data uncovered defects in retinoic acid metabolism in FRDA samples.

Graphical Abstract

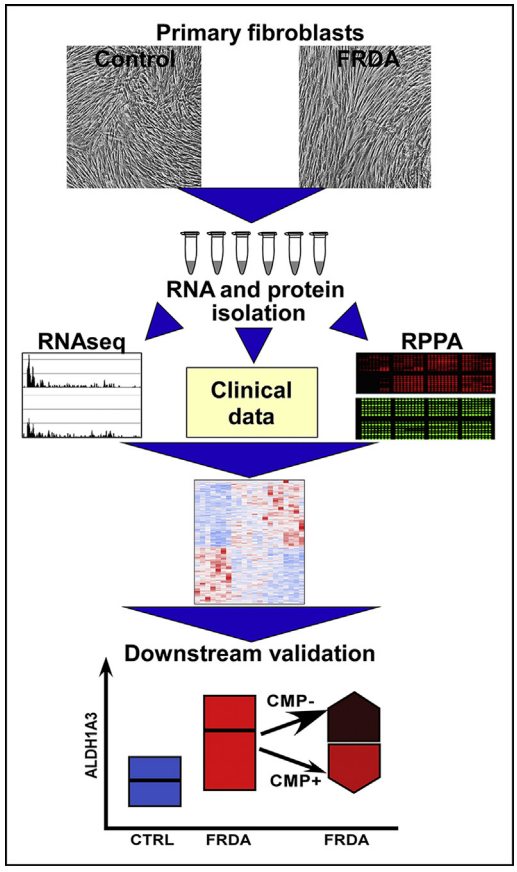

Highlights

- RPPA analyzing Friedreich's ataxia cells reveals changed expression of 30 proteins.
- Integrin expression correlates with hearing loss in Friedreich's ataxia samples.
- Retinol levels are lower in serum of patients with Friedreich's ataxia than controls.

2021, Mol Cell Proteomics *20*, 100094

https://doi.org/10.1016/j.mcpro.2021.100094

Reverse Phase Protein Array Reveals Correlation of Retinoic Acid Metabolism With Cardiomyopathy in Friedreich's Ataxia

Jill S. Napierala[1,*], Kimal Rajapakshe[2], Amanda Clark[1], Yu-Yun Chen[1], Shixia Huang[2], Clementina Mesaros[3], Peining Xu[3], Ian A. Blair[3], Lauren A. Hauser[4], Jennifer Farmer[5], David R. Lynch[4], Dean P. Edwards[2], Cristian Coarfa[2], and Marek Napierala[1,*]

Identifying biomarkers is important for assessment of disease progression, prediction of symptom development, and determination of treatment effectiveness. While unbiased analyses of differential gene expression using next-generation sequencing methods are now routinely conducted, proteomics studies are more challenging because of traditional methods predominantly being low throughput and offering a limited dynamic range for simultaneous detection of hundreds of proteins that drastically differ in their intracellular abundance. We utilized a sensitive and high-throughput proteomic technique, reverse phase protein array (RPPA), to attain protein expression profiles of primary fibroblasts obtained from patients with Friedreich's ataxia (FRDA) and unaffected controls (CTRLs). The RPPA was designed to detect 217 proteins or phosphorylated proteins by individual antibody, and the specificity of each antibody was validated prior to the experiment. Among 62 fibroblast samples (44 FRDA and 18 CTRLs) analyzed, 30 proteins/phosphoproteins were significantly changed in FRDA fibroblasts compared with CTRL cells ($p < 0.05$), mostly representing signaling molecules and metabolic enzymes. As expected, frataxin was significantly downregulated in FRDA samples, thus serving as an internal CTRL for assay integrity. Extensive bioinformatics analyses were conducted to correlate differentially expressed proteins with critical disease parameters (*e.g.*, selected symptoms, age of onset, guanine–adenine–adenine sizes, frataxin levels, and Functional Assessment Rating Scale scores). Members of the integrin family of proteins specifically associated with hearing loss in FRDA. Also, RPPA data, combined with results of transcriptome profiling, uncovered defects in the retinoic acid metabolism pathway in FRDA samples. Moreover, expression of aldehyde dehydrogenase family 1 member A3 differed significantly between cardiomyopathy-positive and cardiomyopathy-negative FRDA cohorts, demonstrating that metabolites such as retinol, retinal, or retinoic acid could become potential predictive biomarkers of cardiac presentation in FRDA.

Friedreich's ataxia (FRDA) is the most prevalent inherited ataxia in humans with a population frequency of 1 to 2:50,000 (1). Most patients with FRDA are homozygous for large expansions of guanine–adenine–adenine (GAA) repeat sequences in intron 1 of the frataxin (*FXN*) gene, whereas a small fraction of patients are compound heterozygotes with an expanded GAA repeat sequence in one *FXN* allele and a missense or nonsense mutation in the other (2). Both types of lesions typically result in reduced levels of FXN protein compared with heterozygous carriers and healthy controls (CTRLs). An inverse correlation exists between FXN protein level and disease severity (1, 3, 4). Characteristic symptoms of FRDA include discoordination, slurred speech, weakness, peripheral neuropathy, and cardiomyopathy (CMP) (5, 6). In addition, optic atrophy, diabetes, and auditory defects are also observed in some patients (7–10).

Importantly, significant heterogeneity in symptom penetration exists within the patient population. Neurological dysfunction occurs in 100% of individuals diagnosed with FRDA, whereas CMP is diagnosed in ~60% of patients, diabetes in ~20%, and ~10 to 20% of patients with FRDA suffer from vision and/or hearing loss (HL) (6). The diversity in age of onset and overall clinical presentation can be in part reconciled by the sizes of the GAA expansions; however, attempts to anticipate symptom development have failed because of the lack of associated biomarkers. In addition to prognostic

From the [1]Department of Biochemistry and Molecular Genetics, University of Alabama at Birmingham, Birmingham, Alabama, USA; [2]Department of Molecular and Cellular Biology, Dan L. Duncan Cancer Center, Baylor College of Medicine, Houston, Texas, USA; [3]Department of Systems Pharmacology and Translational Therapeutics, Perelman School of Medicine, University of Pennsylvania, Philadelphia, Pennsylvania, USA; [4]Division of Neurology, Children's Hospital of Philadelphia, Philadelphia, Pennsylvania, USA; [5]Friedreich's Ataxia Research Alliance, Downingtown, Pennsylvania, USA

*For correspondence: Jill S. Napierala, jsbutler@uab.edu; Marek Napierala, mnapiera@uab.edu.

https://doi.org/10.1016/j.mcpro.2021.100094

biomarkers, a critical element of developing therapeutic strategies is identification of predictive disease biomarkers to allow for managing symptom emergence.

In the past decade, a variety of -omics approaches have been utilized to uncover molecular mechanisms of diseases and identify new biomarkers that would facilitate drug development campaigns and clinical trials. Transcriptome signatures associated with specific disease states can bring to light priority gene expression biomarker candidates and provide critical information about pathogenic mechanisms. Screening methods such as microarrays and bead arrays have been used to define disease signatures, including the FRDA lymphoblast signature (11, 12). The current progress in next-generation sequencing allows us to conduct expression profiling with much greater sensitivity and accuracy. This approach has been employed for large-scale analyses in FRDA research (13, 14), but it is also critical to determine whether transcriptome changes translate to the protein expression differences. In addition, from both therapeutic development and biomarker identification perspectives, it is important to ascertain global proteome differences between FRDA and unaffected CTRL cohorts.

Frequently, high-throughput proteomics studies are conducted by MS methods. These are unbiased and quantitative approaches but are typically limited in resolution to the most abundant proteins in the samples. Thus, identifying DE proteins of lower abundance may be hampered. A few MS-based proteomics studies have been completed thus far in FRDA with limited numbers of samples and predominantly focused on differences between FRDA and CTRL cohorts (15–18).

To complement gene expression profiling approaches, a reproducible and high-throughput method amenable to protein profiling is needed to assess protein expression of biomarker candidates in patient specimens. RPPA technology is an extremely sensitive (pico-to femtomole analyte range), precise (<15% coefficient of variation), and highly efficient (hundreds of samples analyzed in parallel) method for multiplex analysis to identify biomarker candidates and define targets of pathogenesis (19–21). Protein lysates prepared from cultured cells, tissues, or body fluids (among others) are arrayed on a solid phase and probed with an antibody or other affinity reagent with specificity to the target of interest. Furthermore, when spotting the arrays, it is possible to print and store additional slides that can be used for future applications, thus preserving precious patient samples and allowing uniformity when testing new targets and affinity reagents. Biomarker studies comparing protein expression data generated by ELISA and RPPA, conducted with either protein lysates or serum/plasma samples, have consistently demonstrated high correlation between platforms (19, 22, 23), underscoring the reproducibility and clinical compatibility of RPPAs.

Post-translational modifications can also be quantified using this method. RPPA is based on antibody recognition; therefore, its power and precision is limited to proteins for which validated and highly specific antibodies can be identified. The RPPA approach of proteome profiling is frequently utilized in cancer research; our report represents one of the first examples of this method used in the context of neurodegenerative diseases (24).

We employed RPPA to measure changes in protein expression in 44 characterized FRDA primary fibroblast cell lines to define the signatures associated with molecular and clinical features of FRDA and potentially identify prognostic biomarkers. Eighteen fibroblast cell lines derived from unaffected CTRLs were used for comparative analyses. A total of 217 antibodies were used to probe the RPPA. We identified a subset of proteins DE between FRDA and CTRL samples, representing signaling molecules and metabolic enzymes predominantly associated with early apoptotic response and transcription regulation. Furthermore, protein and phosphoprotein expression data were analyzed within the FRDA cohort to identify potential correlations with HL and CMP. Results identified altered expression of integrin protein family members specifically associated with HL in FRDA, whereas defects in the retinoic acid (RA) metabolism pathway were uncovered in FRDA samples that associated with CMP status. These results indicate that retinoid metabolites could become potential predictive biomarkers of cardiac presentation in FRDA.

EXPERIMENTAL PROCEDURES

Patient Samples—Primary Fibroblast Isolation and Culture and Serum Samples

FRDA and CTRL fibroblast cell lines were obtained from the Friedreich's Ataxia Cell Line Repository held at University of Alabama at Birmingham (UAB) and the Coriell Institute. For FRDA primary fibroblast cell line derivation, skin biopsy samples were obtained, and all procedures were conducted in accordance with approvals of Children's Hospital of Philadelphia (CHOP) and UAB Institutional Review Boards (IRBs; CHOP IRB no.: 10-007864; UAB IRB no.: N131204003) (25). The detailed protocol for primary fibroblast line derivation from punch skin biopsy samples has been published (25, 26). Fibroblasts were cultured in high-glucose Dulbecco's modified Eagle's medium (Life Technologies) supplemented with 15% fetal bovine serum (Hyclone) and 1% nonessential amino acids (Life Technologies). For passaging and collection, the cells were incubated in 0.25% trypsin–EDTA (Life Technologies) for 5 min. All fibroblasts were cultured using stringently controlled conditions and reagents. All media and supplements, including fetal bovine serum, were of the same lot number for all cells cultured and collected for this experiment. The cells were harvested for protein isolation when they reached ~80 to 85% confluence. For calculation of population doubling times (PDTs), fibroblasts were seeded at equal densities, cultured under identical conditions, and counted 7 days later. PDTs were calculated using the formula: $PDT = T * \ln 2/\ln(A/A_0)$. For cytotoxicity assays, fibroblasts were plated at equal densities, allowed to settle and grow for 72 h, then fresh media were added with 200 μM hydrogen peroxide (H_2O_2) (or without) for 24 h. Percent cytotoxicity was calculated by measuring lactate dehydrogenase (LDH) activity (CyQUANT LDH Cytotoxicity Assay Kit; Thermo Scientific), according to the manufacturer's recommendations, for the H_2O_2-treated cells compared with the respective untreated CTRL or FRDA cells for each experiment.

Serum samples were collected from patients with FRDA and CTRL subjects enrolled in an ongoing natural history study at CHOP. Serum sample collection procedures were conducted in accordance with approvals of the CHOP IRB (IRB no.: 01-002609) as described (27, 28).

Antibody Validation

All 217 antibodies used to probe RPPA slides were validated by the Antibody-based Proteomics Core at Baylor College of Medicine (BCM) ((20), https://www.bcm.edu/academic-centers/dan-l-duncan-comprehensive-cancer-center/research/cancer-shared-resources/reverse-phase-protein-array). Primary antibodies used to detect human FXN (Abcam; Ab110328) and aldehyde dehydrogenase family 1 member A3 (ALDH1A3) (Novus Biologicals; NBP2-15339) and CYP26B1 (Novus Biologicals; NBP1-33476) on the RPPA were validated by Western blotting of lysates prepared from fibroblast cells stably depleted of each antigen by shRNA. Briefly, fibroblast cells were transduced with lentiviral particles containing shRNA sequences targeting human FXN (FXN MISSION shRNA TRCN0000006137; NM_000144.3-796s1c1 and TRCN0000006138; NM_000144.3-661s1c1), ALDH1A3 (ALDH1A3 MISSION shRNA TRCN0000027144; NM_000693.1-459s1c1), or CYP26B1 (CYP26B1 MISSION shRNA TRCN0000064053; NM_019885.2-242s1c1), or nontargeting shRNA CTRL (MISSION shRNA SHC002), all of which were purchased as plasmid DNA glycerol stocks from Sigma–Aldrich. Fibroblasts were selected with puromycin (2 μg/ml) for 1 week, and then harvested for protein lysate preparation and Western blotting.

RPPA

The RPPA was performed as previously described by the Antibody-based Proteomics Core at BCM with minor modifications (20, 29, 30). Fibroblast cells were detached from the dish by treatment with 0.25% trypsin–EDTA solution, counted, and harvested by centrifugation at 300*g*, 5 min, at 25 °C. Cell pellets were washed twice with ice-cold PBS and centrifuged at 1000*g*, 1 min, at 4 °C. Following the washes, cell pellets were snap frozen in liquid nitrogen and stored at −80 °C until all fibroblast lines were cultured and collected. The fibroblasts were lysed in modified Tissue Protein Extraction Reagent (Pierce) containing a cocktail of protease and phosphatase inhibitors (Roche Life Sciences) at a density of 20,000 cells/μl and kept at 4 °C with mixing for 30 min. Lysates were clarified by centrifugation at 14,000*g*, 15 min, at 4 °C, and supernatants were transferred to fresh tubes followed by protein concentration determination by Bradford assay. Finally, the concentrations of the lysates were adjusted to 0.5 mg/ml, protein sample buffer containing 2.5% 2-mercaptoethanol was added, and the lysates were denatured and printed on nitrocellulose-coated slides (Grace Bio-Labs) using an Aushon 2470 Arrayer (Aushon BioSystems). The samples and CTRL lysates were spotted in an array format of 960 lysates/slide using a 40 pin (185 μm) configuration (total of 2880 spots/slide). Antibodies against 217 total and phosphorylated proteins were used to immunolabel slides using an automated slide stainer Autolink 48 (Dako/Agilent). Each slide was incubated with a unique primary antibody (or antibody diluent as a negative CTRL), followed by incubation with biotinylated secondary antibodies. Finally, primary antibody binding was detected by streptavidin-conjugated IR IRDye680 fluorophore (LI-COR Biosciences). The total protein content for each spotted lysate was quantified by fluorescent staining with Sypro Ruby-Blot Stain (Molecular Probes). Labeled slides were scanned on a GenePix 4400 AL scanner in parallel with negative CTRL slides, and images were analyzed by GenePix Pro 7.0 (Molecular Devices). The fluorescence signal for each spot was determined by subtracting the local slide background signal from the total fluorescence intensity. A previously described group-based normalization method (29, 31) was used to adjust the fluorescent signal for each spot of a sample for varying total protein level, background, and nonspecific labeling. Data quality was evaluated by manual inspection and comparison to CTRL samples. Normalized expression data from the RPPA are provided in supplemental File S1 as the median of three technical replicates per sample.

Experimental Design and Statistical Rationale

DE proteins were identified based on the normalized RPPA data between the FRDA and CTRL groups. A parametric *t* test was used, with significance achieved at $p < 0.05$. Principal component analysis plots and heat maps were generated using the Python scientific library. RNA-Seq data were previously published (14) and deposited into the Gene Expression Omnibus database (GSE104288).

We deployed bioinformatics approaches associating molecular features and clinical variables using techniques pioneered in cancer bioinformatics. We used both parametric (Pearson) and nonparametric (Spearman rank) correlation between proteins or genes of interest and numerical clinical variables; significance was achieved for $p < 0.05$. For categorical clinical variables, we assessed association with genes or proteins using a parametric ANOVA test, with significance achieved for $p < 0.05$. We assessed correlation between molecular features (genes or proteins) across samples using a similar approach. No corrections were implemented for multiple hypothesis testing. Correlation scatter plots were generated using the Python scientific library.

Western Blot

Fibroblasts were harvested by centrifugation (300*g*, 5 min, at 25 °C), and cell pellets were washed once with ice-cold PBS and then centrifuged at 1000*g*, 1 min, at 4 °C. Cells were resuspended in buffer (0.1% NP-40 [Nonidet P-40], 0.25 M NaCl, 5 mM EDTA, 50 mM Hepes [pH 7.5], 0.5 mM DTT, and 0.1% protease inhibitor cocktail [Sigma–Aldrich]) and kept on ice for 20 min for lysis. Suspensions were centrifuged 20,000*g*, 10 min, at 4 °C, and clarified protein lysates were transferred to fresh tubes. Protein concentration was determined by Bradford assay (32), and 50 to 75 μg lysates were separated on 4 to 12% gradient Bis–Tris gels (Life Technologies). Proteins were transferred to nitrocellulose membranes and probed with the following antibodies: ALDH1A3 (Novus Biologicals; NBP2-15339), CYP26B1 (Novus Biologicals; NBP1-33476), FXN (Ab110328; Abcam or GTX54036; Genetex), and GAPDH (EMD Millipore).

Retinol Concentration Measurements

All-*trans* retinol (ROL), 9-*cis* ROL, 13-*cis* ROL, all-*trans* retinal (RAL), 9-*cis* RAL, 13-*cis* RAL, all-*trans* RA, 9-*cis* RA, 13-*cis* RA, and 9,13-*cis* RA were purchased from Santa Cruz Biotechnology. Labeled all-*trans* ROL, all-*trans* RAL, and all-*trans* RA were purchased from Cambridge Isotope Laboratory. Stock solutions were prepared under red light at 1 mg/ml in methanol and stored at −80 °C. Diluted solutions were prepared in methanol and stored in −20 °C. About 500 μl of serum was spiked with 20 μl of retinoid internal standards (ISTD) mixture and vortexed briefly. One thousand microliters of acetonitrile was added to each tube and vortexed for 1 min in the dark, followed by addition of 40 μl of 2 N HCl to the aqueous phase and vortexed for 1 min. Nine milliliters of hexanes was added to each tube and vortexed for 1 min prior to centrifugation for 10 min at 13,000 rpm. The upper organic layer was transferred to a new test tube and dried down under nitrogen. The extracts were reconstituted in 50 μl of methanol and ready for LC–high-resolution MS injection.

The LC–MS analysis of retinoids was conducted using a Q Exactive HF system coupled to Dionex Ultimate 3000. A full scan mode was used for all the retinoids. For quantification, the exact mass ±5 ppm was integrated. Separation was achieved on a BEH C18 column of 50 * 2.1 mm (1.7 μm) after an injection of 10 μl. Solvent A was 0.1%

formic acid, and solvent B was the same in acetonitrile. The column temperature was 20 °C, and the flow rate was 0.4 ml/min. The gradient started from 45% B to 99% B in 10 min, with a 3 min wash and 4 min equilibration. From all the retinoids that were monitored by the LC–MS method, only ROL was present at levels higher than the limit of quantification. All the rest of the retinoids were present at levels higher than the limit of detection (clearly detectable) but lower than the limit of quantification, so the actual values were not reported.

The Q Exactive HF system was equipped with a heated electrospray ionization source operated in the positive ion mode, with a narrow interval of *m/z* 250 to 350 to reduce background. For the analysis, a full scan was utilized with an automatic gain CTRL setting of 1E6, maximum ion time setting of 100 ms, an in-source collision-induced dissociation of 1 eV, and a resolution of 240,000. Operating conditions were spray voltage 3500 V, auxiliary gas heater temperature 100 °C, and heated capillary temperature 320 °C. Nitrogen was used for the sheath gas and auxiliary gas set at 35 and 5 (in arbitrary units), respectively.

Calibration curves were constructed for all analytes using authentic standards and the same amounts of ISTD as used for the serum samples. The area ratio of analyte to ISTD was plotted *versus* the amount of analyte and a linear regression was used to calculate the amount of each analyte. Data analysis was done with Xcalibur software, version 2.6 (ThermoFisher Scientific).

Alternatively, for the data shown in supplemental Fig. S6, ROL was quantified from 100 μl of serum using ultra HPLC/tandem MS, as previously described (33, 34). Metabolites were measured using Agilent 6495 QQQ MS using single reaction monitoring mode. The HPLC column used was Zorbax eclipse XDB C-18, 1.8 micron, 4.6 × 100 mm (Agilent Technologies). The mobile phases used were 0.1% formic acid in water and acetonitrile in mobile phase A and B, respectively. The initial gradient started with 50% of B and maintained until 3 min, and it was ramped in a linear fashion to 80% of B until 13 min, at 13.10 min 50% B, and re-equilibration started until the end of gradient at 20 min. The flow rate used was 0.7 ml/min. The injection volume was 20 μl. Data were acquired using Agilent Mass hunter acquisition software and analyzed using Agilent quantitative analysis software.

RESULTS

High-Throughput Measurement of FXN Protein Expression in Primary Fibroblasts

RPPA was used to interrogate protein expression and post-translational modification changes that are associated with FRDA (Fig. 1*A*). A total of 217 proteins (supplemental Table S1), including phosphorylated species, were profiled in

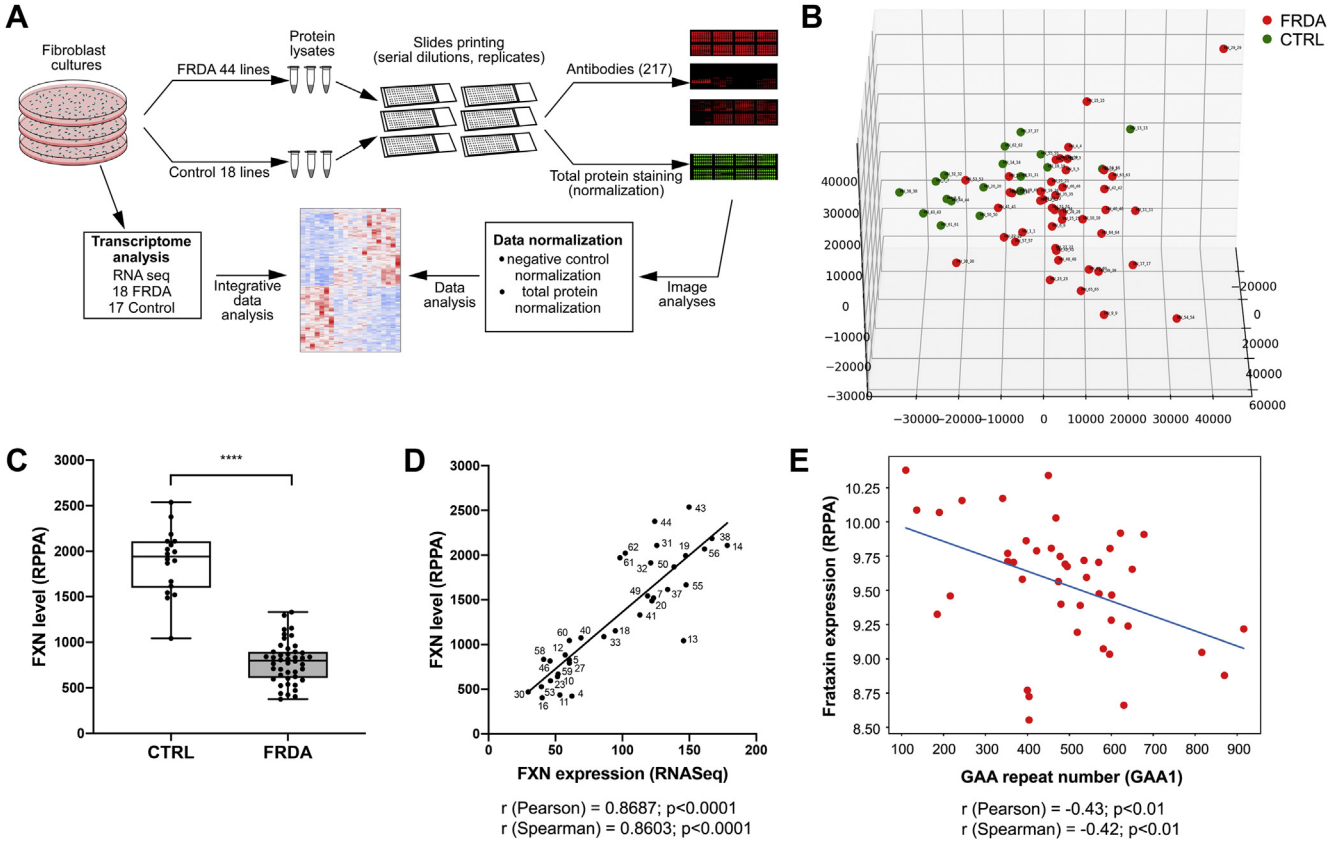

FIG. 1. **High-throughput detection of FXN protein expression in primary fibroblasts.** *A*, schematic of RPPA workflow. *B*, principal component analysis of the 62 fibroblast samples analyzed by RPPA. *C*, normalized FXN protein expression in 18 CTRL and 44 FRDA primary fibroblast cell lines as measured on the RPPA. Significance was determined by Student's *t* test (****$p < 0.0001$). *D*, XY scatter plot and linear regression analysis of FXN expression values as measured by RNA-Seq (*x*-axis) or RPPA (*y*-axis). Results from correlation analyses (Pearson and Spearman) are also presented. *E*, correlation scatter plot displaying FXN protein expression (*y*-axis) *versus* length of GAA1 tract for each FRDA sample. Pearson's and Spearman's correlation coefficients (*r*) were calculated for each comparison. CTRL, control; FRDA, Friedreich's ataxia; FXN, frataxin; GAA, guanine–adenine–adenine; RPPA, reverse phase protein array.

fibroblast samples prepared from 18 apparently healthy CTRL individuals and 44 individuals clinically diagnosed with FRDA. Demographic information for the CTRL and FRDA cohorts is summarized in Table 1, with additional clinical and molecular annotations provided in supplemental Table S2. Sample groups were matched for sex and age of sampling, and molecular characterization of the FRDA fibroblast samples revealed the median lengths for the GAA repeat tracts in *FXN* as 480 (GAA1) and 760 (GAA2) repeat units, with *FXN* mRNA expression reduced by approximately 60% (Table 1). Finally, the specificity of all antibodies included on the array was validated (supplemental Fig. S1) (https://www.bcm.edu/academic-centers/dan-l-duncan-comprehensive-cancer-center/research/cancer-shared-resources/reverse-phase-protein-array).

Principal component analysis of RPPA data showed separation of the FRDA and CTRL sample groups (Fig. 1*B*) indicating significant differences between FRDA and CTRL cellular proteomes. FXN was significantly reduced in FRDA fibroblasts compared with CTRL cells (Fig. 1*C*), and protein expression levels were tightly correlated with *FXN* mRNA expression as determined by next-generation RNA-Seq (14) in the 17 CTRL and 18 FRDA fibroblast lines that were profiled in both experiments (Pearson's $r = 0.866$; $p < 0.0001$; Fig. 1*D* and supplemental Table S2), indicating a strong correlation in FXN measurement between these different platforms. Moreover, a significant inverse correlation was observed between FXN protein expression and the length of the shorter GAA tract (GAA1) (Pearson's $r = -0.43$; $p < 0.01$; Fig. 1*E*), as expected (3, 26). Taken together, these data indicate that RPPA is a robust method for high-throughput FXN protein quantification from a small amount of material and potentially for uncovering underlying disease pathology and identifying protein biomarkers.

Protein Expression Changes in FRDA

Expression values for all 217 proteins/phosphoproteins were compared across the 62 samples to determine DE proteins between the CTRL and FRDA groups. Seventy phospho-specific antibodies were included in the validated set of 217 antibodies, testing a total of 83 unique phosphorylation sites. Thirteen of these antibodies recognize two or more phosphorylation sites on the same protein, and 21 proteins were probed for multiple phosphorylation sites using independent phospho-specific antibodies recognizing single (but unique) phosphorylation sites. Significant changes ($p < 0.05$) were observed in the expression or phosphorylation state of 30 proteins between these sample groups, with ten downregulated and 20 upregulated in FRDA (Fig. 2, *A* and *B*). The protein showing the highest upregulation of expression was ALDH1A3 (Log2 fold change [FC] = 1.74; $p < 0.0001$). In agreement with protein expression data, prior RNA-Seq analyses demonstrated significant upregulation of *ALDH1A3* mRNA levels in FRDA fibroblasts (14). As expected, FXN was the most significantly downregulated protein analyzed (Log2 FC = −1.3; $p < 0.0001$).

The expression values for each of the 30 significantly changed proteins/phosphoproteins were then compared with

TABLE 1
Demographic summary of FRDA and CTRL sample sets

Characteristic		FRDA	CTRL	*p* (FRDA *versus* CTRL)
Sample number		44	18	
Sex	Females	55%	50%	
	Males	45%	50%	
Age at sampling (y)	Minimum	13	1	
	Maximum	70	64	
	Median	31	26.5	ns; $p = 0.267$
Age of onset (y)	Minimum	4		
	Maximum	43		
	Median	14		NA
Cardiomyopathy	Present (+)	17		
	Absent (–)	21		
	Undetermined	6		
GAA1 length	Minimum	110		
	Maximum	916		
	Median	480		NA
GAA2 length	Minimum	216		
	Maximum	1470		
	Median	760		NA
FXN mRNA (RNA-Seq)	Minimum	0.22		
	Maximum	0.83		
	Median	0.41		$p = 5.25E-18$

NA, not available; ns, not significant.
Clinical and molecular data for FRDA and CTRL subjects from which fibroblast cell lines were derived.

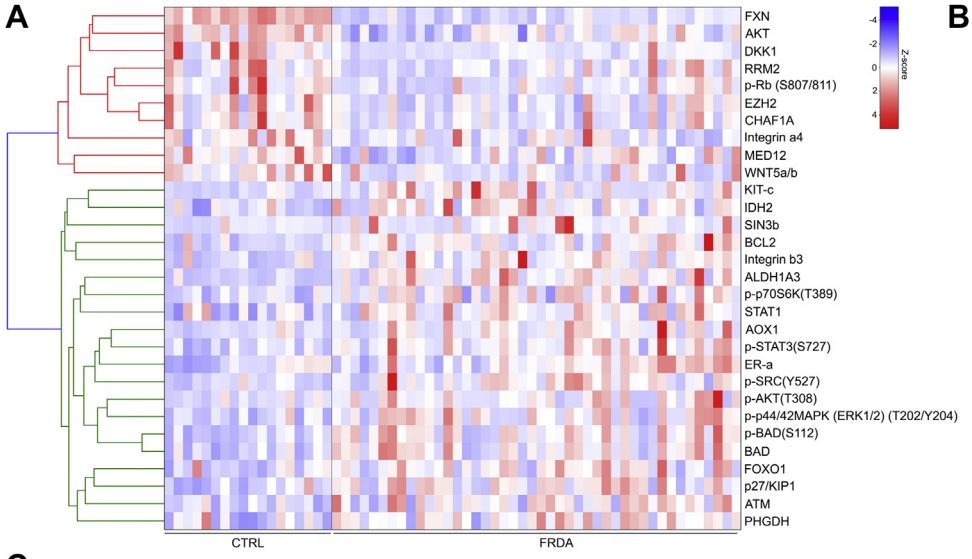

B

Protein	Log2 FC (FRDA/CTRL)	p value
ALDH1A3	1.74	3.511E-07
Integrin b3	1.53	5.1843E-06
KIT-c	1.15	0.000331183
p-p44/42MAPK (Erk1/2) (T202/Y204)	1.08	0.000227171
PHGDH	0.67	0.00056711
AOX1	0.62	0.001827877
FOXO1	0.6	0.004708188
p-BAD (S112)	0.6	6.6515E-06
BCL2	0.59	0.000147356
ER-a	0.57	0.002365321
p-AKT (T308)	0.56	0.026510613
BAD	0.54	3.56643E-05
p27/KIP1	0.54	0.000154109
p-SRC (Y527)	0.52	0.000379789
p-STAT3 (S727)	0.51	6.09673E-05
IDH2	0.47	0.0011811
STAT1	0.45	0.000852744
p-p70S6K (T389)	0.44	0.008695076
ATM	0.37	0.002303593
SIN3b	0.35	0.034501826
MED12	-0.36	0.00417343
AKT	-0.38	2.41676E-05
EZH2	-0.45	0.007522466
Integrin a4	-0.46	0.041578231
RRM2	-0.53	0.02518338
p-Rb (S807/811)	-0.54	0.004208249
CHAF1A	-0.64	0.00432089
DKK1	-0.7	1.40019E-05
WNT5a/b	-1.06	0.000596657
FXN	-1.3	0

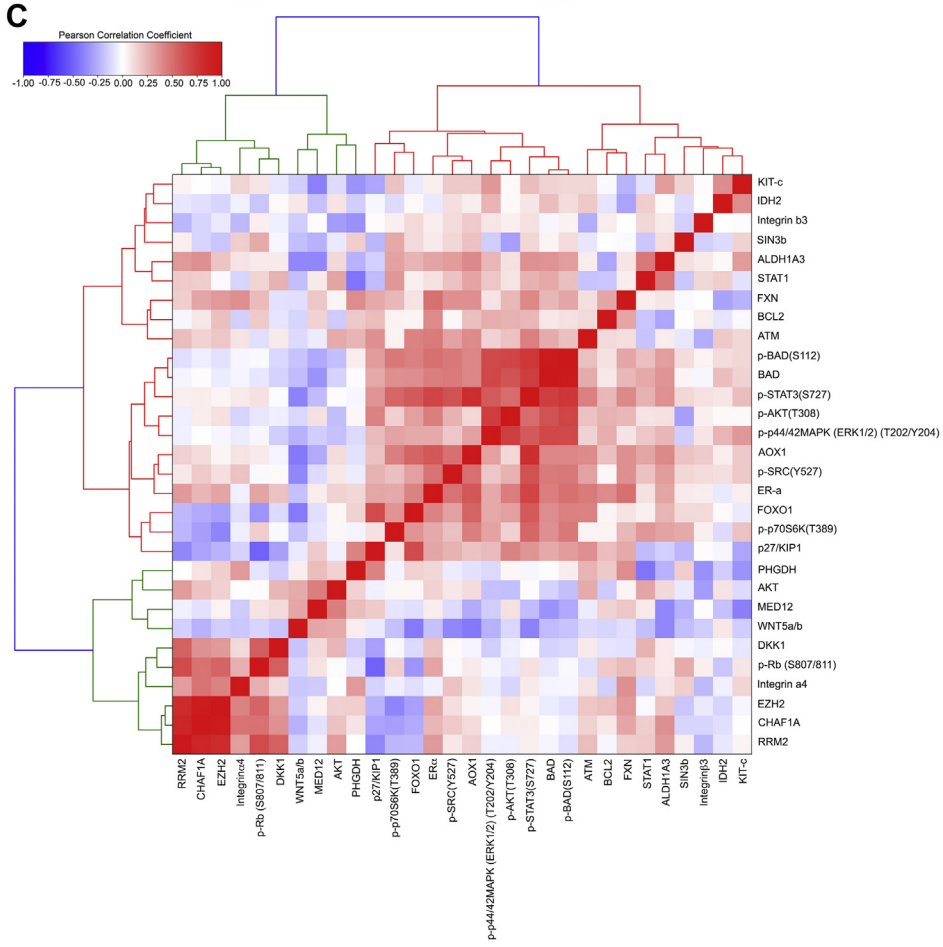

FIG. 2. **Differential protein expression between CTRL and FRDA samples.** *A*, heat map illustrating expression levels of 30 proteins identified as significantly different ($p < 0.05$) between FRDA and CTRL groups. Shades of *blue* indicate lower expression, whereas shades of *red* indicate increased protein levels. *B*, a summary of Log2 FC expression ratios along with *p* values is provided. Proteins are listed in descending order based on expression change; shades of *red* indicate increased expression in FRDA, and shades of *blue* indicate reduced expression in FRDA. *C*, Pearson correlation coefficients were calculated for significantly changed proteins using their RPPA expression values in FRDA samples. Proteins and their correlation coefficients were organized by hierarchical clustering and are shown by the heat map (correlation matrix). The color key indicates shades of *red* for positive correlation coefficients ($r > 0$) and shades of *blue* for negative correlation coefficients ($r < 0$). CTRL, control; FC, fold change; FRDA, Friedreich's ataxia; RPPA, reverse phase protein array.

TABLE 2
Expression of significantly changed proteins (CTRL versus *FRDA)* versus *molecular and clinical features of FRDA*

Protein	Sampling age	Age of onset	FARS score	GAA1	GAA2	FXN mRNA (RNA-Seq)
ALDH1A3	0.25	0.18	−0.17	−0.06	−0.02	0.06
Integrin b3	0.12	0.19	−0.24	−0.16	−0.06	0.02
KIT-c	−0.17	**−0.31**	0.22	**0.33**	0.20	−0.28
p-p44/42MAPK (ERK1/2) (T202/Y204)	0.05	−0.02	0.09	0.05	0.04	−0.08
PHGDH	0.05	0.07	−0.12	−0.09	−0.07	**0.40**
AOX1	0.26	**0.37**	**−0.33**	−0.24	0.11	**0.34**
FOXO1	0.08	0.26	**−0.36**	−0.26	−0.17	0.18
p-BAD (S112)	−0.04	−0.01	−0.18	−0.04	−0.04	0.03
BCL2	−0.13	−0.22	0.25	0.23	0.16	−0.08
Era	−0.01	0.05	0.07	0.04	0.13	−0.01
p-AKT (T308)	0.04	0.03	0.07	0.10	−0.08	−0.04
BAD	−0.03	−0.03	−0.17	−0.05	0.02	−0.05
p27/KIP1	0.02	0.09	**−0.32**	**−0.32**	**−0.30**	0.23
p-SRC (Y527)	−0.10	0.06	**−0.45**	−0.03	0.17	0.11
p-STAT3 (S727)	0.11	0.18	−0.13	−0.08	0.03	0.12
IDH2	−0.03	**−0.32**	0.17	**0.33**	0.27	**−0.42**
STAT1	0.09	0.09	−0.05	−0.04	0.23	−0.03
p-p70S6K (T389)	−0.05	0.01	−0.04	−0.25	0.02	0.12
ATM	0.07	0.14	−0.01	−0.02	0.17	−0.07
SIN3b	−0.05	−0.05	−0.01	0.08	0.10	0.09
MED12	−0.16	−0.04	0.06	0.08	−0.07	0.06
AKT	0.06	0.20	0.06	0.09	0.26	0.01
EZH2	0.24	0.19	0.22	0.22	0.08	0.05
Integrin a4	0.10	**0.34**	**−0.38**	−0.09	0.01	**0.43**
RRM2	0.25	0.24	0.23	0.18	0.17	−0.03
p-Rb (S807/811)	0.09	0.06	**0.33**	0.20	0.19	−0.01
CHAF1A	0.25	0.18	0.14	0.22	0.14	0.03
DKK1	0.01	**0.33**	0.01	0.15	**0.30**	−0.08
WNT5a/b	−0.16	−0.18	0.14	0.07	−0.12	−0.19
FXN	0.22	**0.30**	−0.24	**−0.43**	−0.23	*0.62*

Pearson correlation coefficient values (*r*) are shown for each comparison. Values of r ≥ |0.3| are highlighted in *bold* and r ≥ |0.5| are highlighted in *italics*.

clinical and molecular features of FRDA: age of onset, Functional Assessment Rating Scale (FARS) score, number of repeats in GAA1, number of repeats in GAA2, and RNA expression by RNA-Seq (Table 2). The protein most strongly correlated with age of disease onset was the aldehyde oxidase 1 (AOX1) (r = 0.37). AOX1 protein expression also inversely correlated with FARS score (r = −0.33), a measure of disease progression, suggesting AOX1 levels as a potential monitoring biomarker for FRDA. The strongest correlations observed for FARS scores were with p-SRC(Y527) (r = −0.45) and Integrin a4 (r = −0.38), suggesting their potential also as prognostic markers. Importantly, no protein expression changes were associated with sampling age (Table 2) or sex (supplemental Table S3), indicating that these variables did not confound our analyses.

As an approach to uncover additional proteins potentially associated with various clinical presentations of FRDA, all 217 proteins/phosphoproteins profiled on the RPPA, irrespective of their differential expression status between FRDA and CTRL cohorts, were analyzed for correlation with clinical features of FRDA (supplemental Fig. S2). Continuous variables, including age of onset, FARS, FXN protein expression by RPPA, and sampling age, were considered. Expression of five proteins showed a significant correlation with sampling age (p-p70S6K (T412), LDH A, hypoxia-inducible factor 1 subunit alpha, p-AuroraA (T288)/B (T232)/C (T198), and cyclooxygenase-2) (supplemental Fig. S2*A*), indicating that any observed associations with these proteins might not necessarily be related to FRDA pathophysiology. Expression of various integrin receptor subunits was significantly associated with age of onset (integrin a4), FARS score (integrins a4, a5, aV, and b1), FXN protein expression (integrins a4 and b3) (supplemental Fig. S2, *B–D*), suggesting a role for integrin signaling in disease manifestation and progression. Particularly, expression of integrin a4, which also is significantly downregulated in FRDA compared with CTRL samples (Fig. 2*B*), was directly correlated with age of onset (Pearson's r = 0.34; supplemental Fig. S2*B*) and FXN protein expression (Pearson's r = 0.39; supplemental Fig. S2*D*) and inversely correlated with FARS score (Pearson's r = −0.38; supplemental Fig. S2*C*), indicating that this protein may be an important player in the molecular pathology of FRDA.

Correlation Matrix Identifies Clusters of Coregulated Proteins

To determine if any coregulatory mechanisms exist for the 30 proteins/phosphoproteins significantly changed in FRDA, a Pearson correlation matrix was calculated based on protein expression values across FRDA samples (Fig. 2*C*). Hierarchical clustering revealed a major cluster consisting of five proteins/phosphoproteins (p-BAD [S112], BAD, p-STAT3 [S727], p-AKT [T308], p-p44/42MAPK [ERK1/2 (T202/Y204)]) and a second cluster of three (RRM2, CHAF1A, and EZH2). The first group contains proteins functioning predominately in the initial phases of the intrinsic apoptosis pathway (35–37). All these proteins are significantly upregulated in FRDA cells (Fig. 2*B*), which might indicate a disruption in balance of early proapoptotic and antiapoptotic signaling. Interestingly, expression of late apoptosis effectors, such as caspase 3, cleaved caspase 3, and cleaved caspase 7 (36, 38) (supplemental Table S1), is not different between the FRDA and CTRL cohorts (supplemental Fig. S3, *A*–*C*). In addition, no changes were observed in growth characteristics between FRDA and CTRL fibroblasts in the conditions used to culture these cells for RPPA analyses (PDTs: CTRL = 31.3 ± 4 h, FRDA = 34.5 ± 4 h) (supplemental Fig. S3*D*). This suggests that FRDA cells cultured in optimal conditions are primed for apoptosis; however, when unchallenged, the process of programmed cell death is not fully initiated. In agreement with previous findings, FRDA fibroblasts showed increased sensitivity compared with CTRL fibroblasts when treated with H_2O_2, as demonstrated by higher measured cytotoxicity (supplemental Fig. S3*E*) (39, 40).

The second cluster includes three proteins associated with DNA metabolism (synthesis, repair, and chromatin modification) (41–43). Expression levels of all these proteins are decreased in FRDA cells and may indicate a global trend toward decreased DNA/RNA metabolic activity caused by reduced FXN levels, confirming our initial observation based on comprehensive FRDA transcriptome analyses (14).

Phosphorylation State Changes of Key Signaling Molecules in FRDA

We next analyzed changes in phosphorylation states associated with FRDA by calculating the phospho-to-total protein ratios (24) for 49 unique phosphorylated proteins probed on the RPPA. Expression data from antibody pairs (phosphorylated and nonphosphorylated) recognizing only the same protein targets (*e.g.*, matching Swiss IDs) were analyzed. All antibodies are listed in supplemental Table S1, with phospho-specific antibodies denoted by the "phospho" prefix and the 49 phospho-specific antibodies included in the phospho-ratio analysis indicated by gray shading. Of these, 13 phosphoprotein/protein ratios were significantly different between FRDA and CTRL samples, with five showing upregulation and eight being reduced in FRDA (Fig. 3). Despite overall decreased levels of the AKT kinase in FRDA samples (Fig. 2), phosphorylation at two activating sites (T308 and S473) is enriched (Fig. 3). Reduced levels of phosphorylated species of BAD (at S136 and S155) and BCL2 (T56 and S70) proteins were observed in FRDA compared with CTRL cells (Fig. 3), whereas the unmodified forms of these proteins were upregulated in FRDA samples

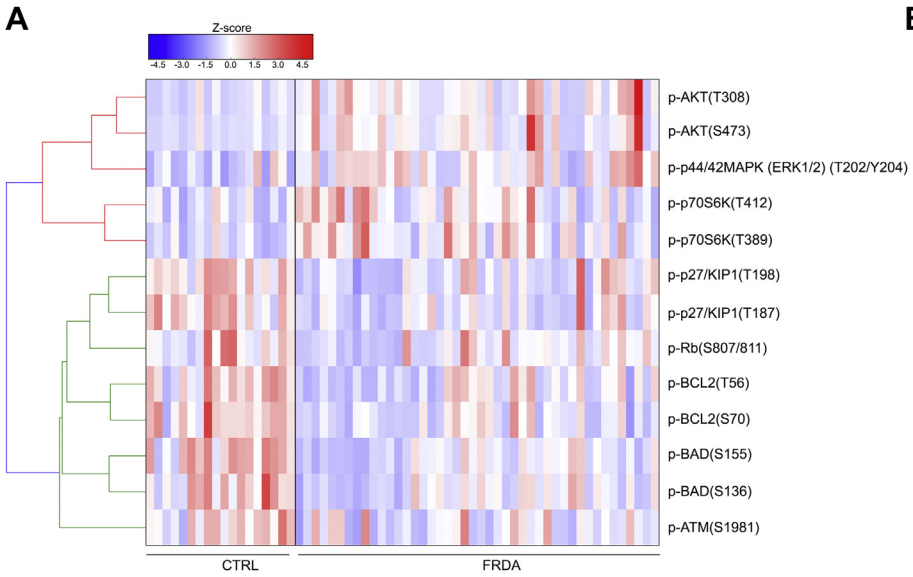

B

p-Protein	Log2 FC (FRDA/CTRL)	p value
p-p44/42MAPK(ERK1/2)(T202/Y204)	1.12	9.486E-05
p-AKT(S473)	1.01	0.0075794
p-AKT(T308)	0.92	0.0013282
p-p70S6K(T389)	0.76	0.0011316
p-p70S6K(T412)	0.43	0.0113604
p-ATM(S1981)	-0.37	0.0051714
p-Rb(S807/811)	-0.39	0.0421382
p-BAD(S136)	-0.42	9.492E-05
p-p27/KIP1(T198)	-0.46	0.0003407
p-BAD(S155)	-0.61	7.741E-07
p-BCL2(S70)	-0.64	4.712E-05
p-p27(T187)	-0.67	6.136E-05
p-BCL2(T56)	-0.68	0.000566

FIG. 3. **Altered phospho-to-total protein ratios in FRDA fibroblasts.** *A*, heat map displaying expression changes of phosphorylated forms *versus* total level of proteins that were significantly different ($p < 0.05$) between FRDA and CTRL samples. *B*, a summary of the 13 significantly changed phosphoproteins with their calculated Log2 FC in expression and associated *p* value. CTRL, control; FC, fold change; FRDA, Friedreich's ataxia.

(Fig. 2, *B* and *C*), again suggesting an altered homeostasis in apoptosis signaling. Moreover, levels of p27 (KIP1) phosphorylated at both T187 and T198 are decreased in FRDA cells (Fig. 3), in agreement with the inverse relationship that exists for the phosphorylation status and total levels of p27/KIP (Fig. 2, *A* and *C*) (44, 45). This result also indicates a potential effect of FXN downregulation on cell cycle progression. Taken together, these protein expression and phosphorylation changes suggest that FRDA cells are "stress-primed" and render FXN-depleted cells sensitive to insults that are tolerated by CTRL (supplemental Fig. S3).

Protein Expression Signature Correlated With HL in FRDA

One of the most critical tasks in combating a heterogeneous disease such as FRDA is identifying predictive biomarkers for the nonfully penetrant symptoms, such as hearing and vision impairment or CMP (46). To identify a potential protein expression signature associated with HL, the FRDA sample group was divided into patients who had been diagnosed with HL prior to skin biopsy (HL+; n = 14) or those without (HL–; n = 24) (supplemental Table S2), and expression of all 217 proteins/phosphoproteins was analyzed for differences between these groups. The expression of four proteins was found to be significantly decreased in patients with FRDA diagnosed with HL: HER2/c-ERBB2, CTBP2, integrin b3, and integrin a5 (Fig. 4*A*), with integrin a5 showing the most significant FC between the groups (Fig. 4*B*). Analysis of RNA-Seq data showed similar mRNA expression for the *ERBB2*, *CTBP2*, *ITGB3*, and *ITGA5* genes between FRDA HL+/– samples, suggesting post-translational mechanisms are likely responsible for downregulating levels of these four proteins (supplemental Fig. S4).

In addition to lower expression of integrin a5 in FRDA patients with HL, expression of both integrin a5 and b1 was inversely correlated with FARS scores (Fig. 4, *C* and *D*). Integrin a5 heterodimerizes with integrin b1 (a5/b1) to form a cell surface receptor for fibronectin (47, 48). Moreover, integrin aV and integrin b3 also heterodimerize (aV/b3) and serve as receptors for fibronectin and vitronectin (48, 49). Decreased integrin b3 expression was associated with HL in FRDA (Fig. 4, *A* and *B*), whereas decreased integrin aV expression was correlated with increased FARS scores (Fig. 4*E*). Taken together, these data suggest a potential for altered integrin signaling in HL and overall progression in FRDA.

Protein Expression Signature Correlated With CMP in FRDA

CMP is a leading cause of death in FRDA (50); therefore, efforts to improve cardiac function as well as to identify presymptomatic markers of CMP are of critical importance.

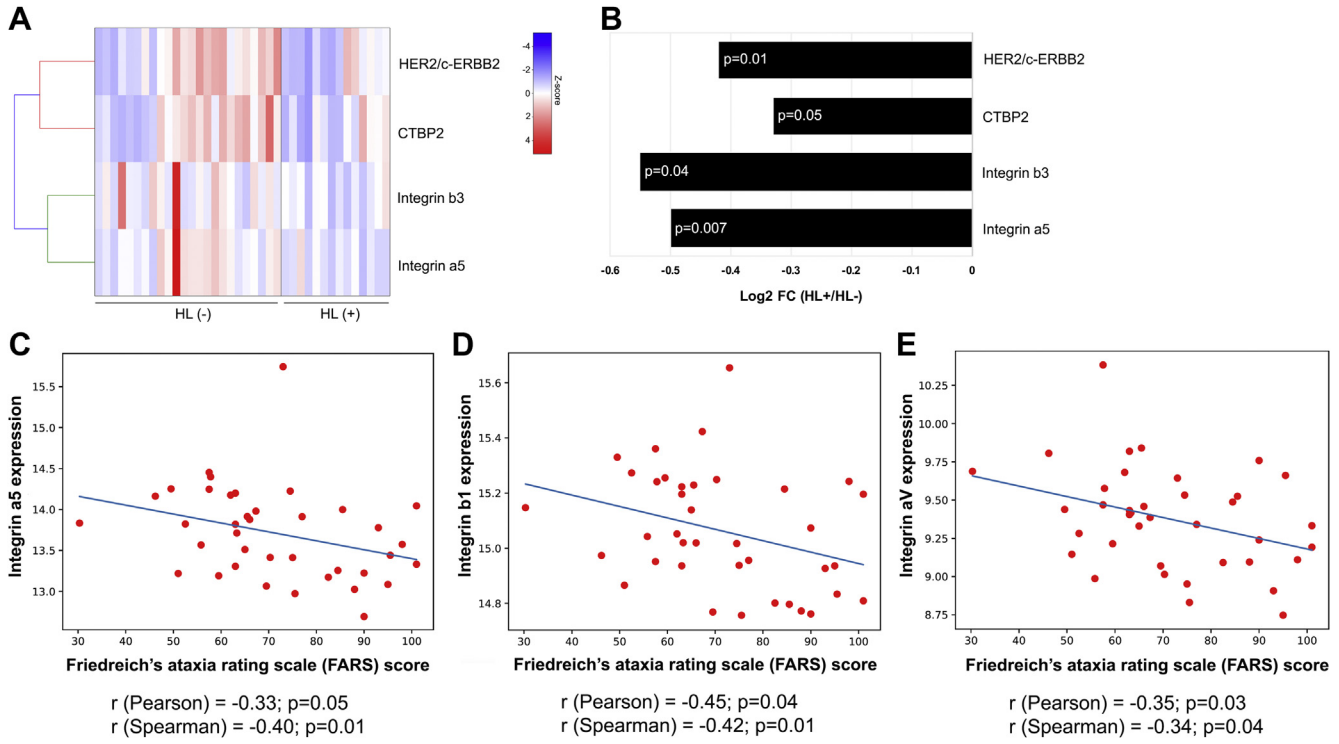

FIG. 4. **Proteins significantly changed in patients with FRDA diagnosed with hearing loss (HL).** *A*, heat map illustrating differentially expressed proteins ($p < 0.05$) between FRDA HL+/– groups. *B*, bar plot of Log2 FC ratios for HL+/HL– FRDA groups. *C–E*, correlation scatter plots displaying integrin a5 (*C*), integrin b1 (*D*), or integrin aV (*E*) protein expression *versus* FARS scores for all FRDA samples analyzed by RPPA. Pearson and Spearman correlation coefficients (*r*) were calculated for each comparison. FARS, Functional Assessment Rating Scale; FC, fold change; FRDA, Friedreich's ataxia; HL, hearing loss; RPPA, reverse phase protein array.

To determine a protein expression signature associated with CMP, the FRDA sample group was divided into patients who had been diagnosed with hypertrophic CMP (CMP+; n = 17) at the time of skin biopsy or those reported without (CMP–; n = 21) (Table 1 and supplemental Table S2). Expression of all 217 proteins was analyzed for comparison between the two groups. Five proteins were significantly changed, with most showing decreased expression in FRDA CMP+ samples (Fig. 5, *A* and *B*). The most significant difference in expression was observed for the ALDH1A3 (Log2 FC = −0.98; p = 0.006). We also analyzed potential relationships between expression of the five proteins with

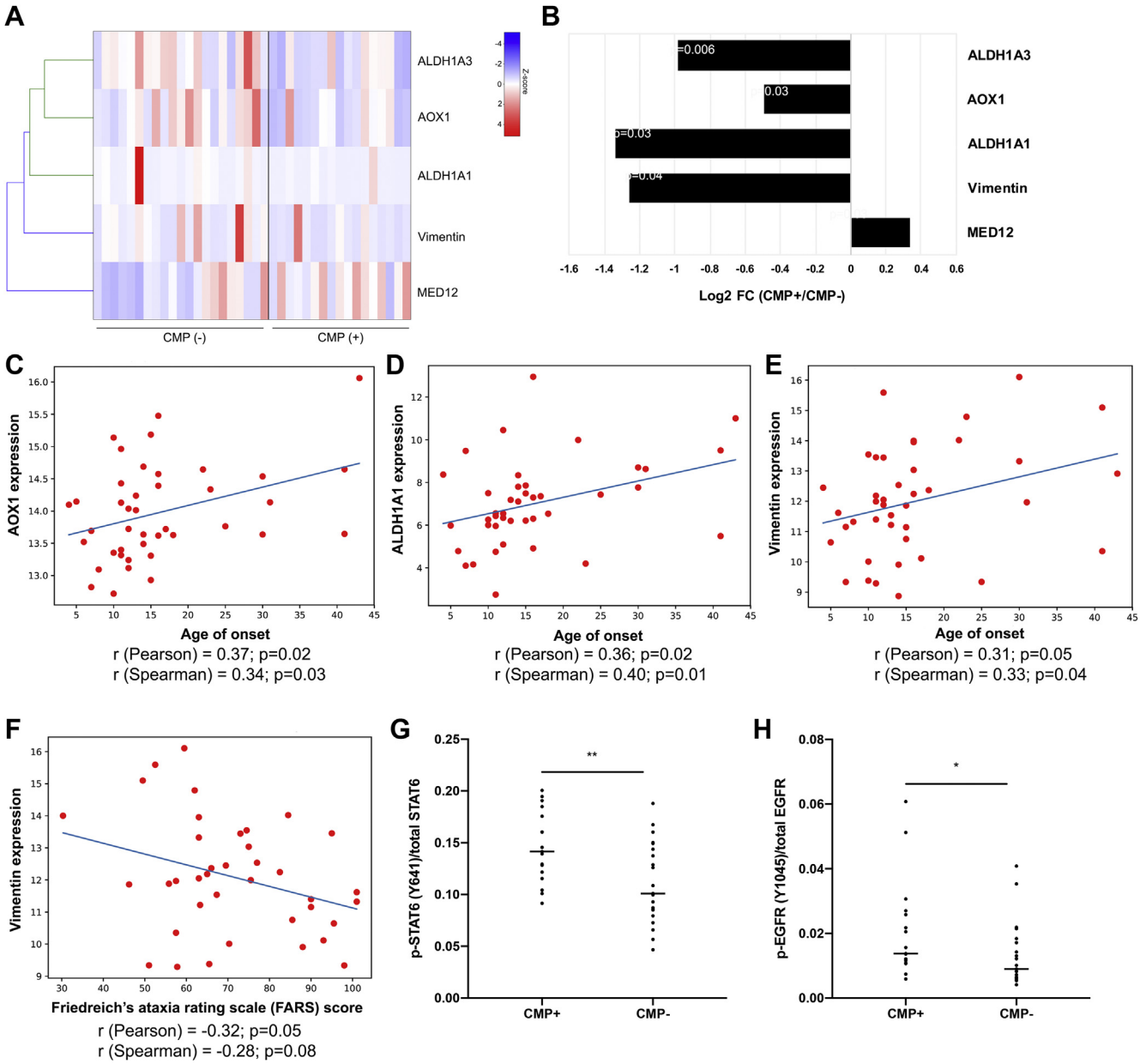

FIG. 5. **Proteins significantly changed in patients with FRDA diagnosed with cardiomyopathy.** *A*, heat map illustrating differentially expressed proteins ($p < 0.05$) between FRDA CMP+/– groups. *B*, bar plot of Log2 FC ratios for FRDA CMP+/– groups. *C–E*, correlation scatter plots displaying AOX1 (*C*), ALDH1A1 (*D*), or vimentin (*E*) protein expression *versus* age of disease onset for all FRDA samples analyzed by RPPA. Pearson's and Spearman's correlation coefficients (*r*) were calculated for each comparison. *F*, correlation scatter plot displaying vimentin protein expression *versus* FARS score for all FRDA samples analyzed by RPPA. Pearson's and Spearman's correlation coefficients (*r*) were calculated. *G* and *H*, phospho-to-total protein ratios were calculated between FRDA CMP+ and CMP– samples and plotted for p-STAT6 (Y641) and pEGFR (Y1045). *Asterisks* indicate significant differences: $^{**}p < 0.01$ and $^{*}p < 0.05$, using Student's *t* test. CMP, cardiomyopathy; FARS, Functional Assessment Rating Scale; FC, fold change; FRDA, Friedreich's ataxia; RPPA, reverse phase protein array.

demographic and clinical features of FRDA. Expression of AOX1, ALDH1A1, and VIM was positively associated with age of onset (Fig. 5, *C–E*), whereas AOX1 and VIM expression were inversely related to disease progression (FARS score) (Table 2 and Fig. 5*F*). Finally, by analyzing the phosphorylation ratio data generated by RPPA, we found that levels of phosphorylated STAT6 (Y641) and epidermal growth factor receptor (Y1045) were enriched relative to the unmodified forms of these proteins in FRDA CMP+ samples compared with the CMP– group (Fig. 5, *G* and *H*), suggesting altered activation of their respective signaling networks, despite similar levels of the unphosphorylated forms of these proteins between the groups.

Interestingly, analysis of RNA-Seq data revealed that ALDH1A3 levels were significantly lower in CMP+ samples (in agreement with protein levels), but mRNA expression of the other CMP-associated proteins was not significantly different between the groups (supplemental Fig. S5). This indicates that altered regulation of ALDH1A3 levels likely plays a role in FRDA pathology.

Altered Retinoid Metabolism Associated With FRDA CMP Status

ALDH1A3 protein level was observed as significantly increased across the FRDA sample group compared with the CTRL group, albeit at variable levels (Figs. 2*A* and 6*A*). Furthermore, patients with FRDA without a diagnosis of CMP tended to have higher levels of ALDH1A3 than those diagnosed with CMP (Figs. 5 and 6*A*), suggesting that higher expression of this enzyme may have a protective role under conditions of decreased FXN levels. To confirm the RPPA measurement of ALDH1A3 protein levels in FRDA fibroblasts, Western blots were performed on lines selected for low (3 and 4), medium (6 and 39), and high (51) ALDH1A3 expression. The results correspond to levels observed by RPPA and independently validate ALDH1A3 protein expression in FRDA cells as well as CTRL cells (Fig. 6, *A–C*). Western blotting also confirms that FXN levels are uniformly reduced in all FRDA samples, as expected (Fig. 6, *B* and *D*). *ALDH1A3* mRNA expression as measured by RNA-Seq was tightly associated with protein level as determined by RPPA in each sample (Pearson's $r = 0.6086$; $p = 0.016$) and showed significantly lower expression in FRDA CMP+ samples (Fig. 6, *A* and *E*). Moreover, we observed a fourfold "correction" of *ALDH1A3* expression in FRDA CMP+ induced pluripotent stem cell–differentiated cardiomyocytes (FRDA line 58) from which expanded GAA repeats had been removed from one allele (52) (Fig. 6*F*).

ALDH1A3 is an intracellular cytoplasmic enzyme, and measuring its level would be rather difficult in a clinical setting. ALDH1A3 catalyzes the irreversible oxidation of retinaldehyde (retinal) to RA (53, 54). ROL (vitamin A), the precursor of RAL, circulates in the bloodstream as the transport retinoid for delivery to various tissues and can be measured in serum (55, 56). Therefore, serum ROL levels were quantified as a surrogate for retinoid metabolism and found to be significantly decreased in FRDA compared with CTRL samples (360.1 ± 141.3 ng/ml *versus* 681.3 ± 294 ng/ml, respectively, $p = 0.0041$; Fig. 6*G*). A second independent study confirmed the significant reduction in ROL levels in FRDA compared with CTRL serum samples (supplemental Fig. S6). Finally, separating the FRDA group into samples obtained from CMP+ or CMP– individuals revealed an increase, although not significant, of serum ROL in CMP– compared with CMP+ groups (436.8 ± 162.7 ng/ml *versus* 283.4 ± 57.49 ng/ml, respectively, $p = 0.054$; Fig. 6*H*). Taken together, these results suggest that serum ROL levels could be evaluated as a potential predictive biomarker for the development of CMP in individuals diagnosed with FRDA.

DISCUSSION

Quantitative proteomics analyses of disease states offer significant advantages over transcriptome studies. DE mRNAs may not directly reflect protein changes and consequent influences on phenotype. Frequently, cellular compensation mechanisms or redundant pathways can counteract transcriptome differences and alleviate potential changes at the proteome level. Another significant advantage of proteomics approaches is the possibility of detecting not only DE proteins but also changes in their post-translational modifications that may better represent protein activity. Although significant progress has been made to increase sensitivity and robustness of protein expression profiling approaches, especially in detecting low-abundance proteins, most proteomic-based methods are not yet comparable to contemporary methods used to define transcriptome signatures.

Thus far, only a few proteomics studies were reported using FRDA patient–derived material, performed using small numbers of patient samples and using MS-based approaches (15–18). Here, for the first time, we compared protein expression signatures of a large cohort of FRDA primary fibroblasts, known to express molecular hallmarks of the disease, with a representative group of age- and sex-matched CTRL cells. To gain on sensitivity and throughput, we selected RPPA as our method and profiled expression of 217 proteins/phosphoproteins in a total of 62 primary cell lines. Results showed that expression of 30 proteins was significantly changed in FRDA fibroblasts compared with CTRL cells ($p < 0.05$). In addition to changes at the protein level, the phosphorylation status of a subset of proteins differed between the FRDA and CTRL cohorts. Detailed clinical information accompanying the FRDA samples allowed us to identify relationships between protein expression levels and clinical features of the disease, including HL and CMP.

Results of our RPPA analyses contribute toward deciphering the disease mechanism and identification of potential FRDA biomarkers. Correlation matrix data highlighted expression changes of groups of proteins potentially acting in the same pathway. One of the two clusters revealed by this

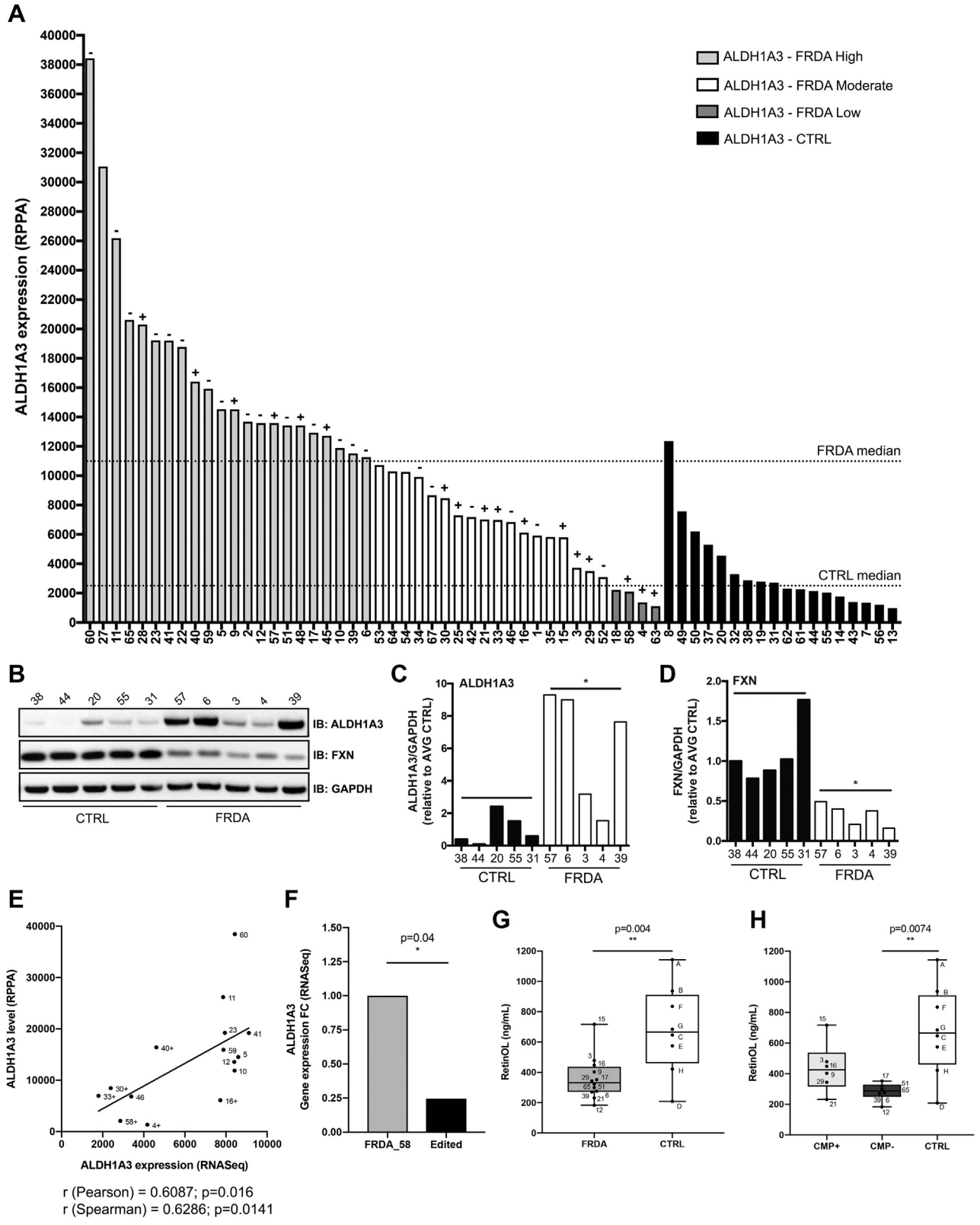

FIG. 6. **Retinoid metabolism is altered in FRDA.** *A*, bar graph depicting ALDH1A3 protein expression in all fibroblast samples as determined by RPPA with samples stratified by expression level (FRDA—high [*gray*], FRDA—moderate [*white*], FRDA—low [*dark gray*], and CTRL [*black*]). *Dotted lines* indicate ALDH1A3 average protein expression for FRDA and CTRL sample groups. FRDA patients with and without cardiomyopathy (CMP) are denoted by a (+) or (–), respectively. *B*, Western blot on fibroblast whole cell lysates selected from ALDH1A3 high-, moderate-, or low-

analysis showed changes in the apoptosis-related proteome in FRDA cells. This analysis was supported by differential expression of phosphorylated forms of several apoptosis-regulating proteins including AKT, BCL, and BAD. While induction of apoptosis has been reported in various FRDA models, especially those generated by sudden externally induced depletion of FXN (*i.e.*, *via* siRNA or shRNA), these changes were typically associated with decreased cell viability or proliferation (51, 57–59). Moreover, appearance of advanced or late apoptosis markers, such as increased Ca^{2+} release and caspase cleavage, was observed in these studies (57–59).

No differences in expression of late apoptosis markers were detected between FRDA and CTRL cells in our study. In addition, when FRDA and CTRL fibroblasts were cultured in identical conditions, no gross growth differences that could be attributed to the FRDA status were observed. Thus, based on protein profiling data and changes in expression of early proapoptotic markers, including key apoptotic sensors such as AKT, BCL, or BAD, we define a phenotype of FRDA primary cells as "susceptible to intrinsic apoptosis." The apoptosis-primed signature defined by our protein expression data in FRDA fibroblasts is consistent with results of a previous study demonstrating increased sensitivity of FRDA fibroblasts to acute oxidative stress that could be prevented by pretreatment of the cells with antiapoptotic agents (39). These results strongly suggest that the low level of FXN expression in patient cells renders them vulnerable to any potential further insult. Somatic expansion of the GAA repeats resulting in the lowering of *FXN* expression, accumulation of ROS, or cellular age–related accumulation of mitochondrial/nuclear genome damage and any other cellular stressor can tip the fragile balance and promote further changes in the apoptotic program. This discovery opens a potential therapeutic opportunity at the cellular level by presymptomatically targeting the metabolism of a cell to delay preapoptotic changes and defer degenerative processes.

A second cluster identified in our RPPA data included three proteins functionally involved in DNA/chromatin metabolism. Interestingly, RRM2, CHAF1A, and EZH2 were all downregulated in the FRDA cohort. Although chromatin changes reported in FRDA were localized to the *FXN* gene, specifically proximal to the GAA repeats (60–64) without spreading toward neighboring upstream or downstream genes (26), transcriptome profiling of FRDA cells indicates significant global effects on pathways governing gene expression (14, 65). Chromatin modifiers such as histone methyltransferases (EZH2) or chromatin assembly proteins (CHAF1) may represent the effectors responsible for global changes of the chromatin environment in FRDA cells contributing to the subsequent transcriptome remodeling observed in FRDA cells.

Hearing impairment observed in patients with FRDA has been studied from a clinical perspective (10, 66–69). A consensus exists that the ability to detect sound is relatively unaffected in FRDA while auditory processing is compromised as a consequence of auditory neuropathy (10, 67). On the other hand, no data exist related to the molecular mechanisms or pathways contributing to the development of hearing deficits in FRDA. Also, it is unclear why this symptom affects only a small subset of the patients. Here, we identified four proteins: HER2/c-ERBB2, CTBP2, integrin b3, and integrin a5 that were significantly downregulated in patients with FRDA diagnosed with HL.

The downregulation of integrins in this cohort of patients with FRDA is especially interesting as integrin b3 has been associated with differentiation of inner ear cells (70). Also, appropriate expression of integrins is necessary for organization and function of hair cells in the mammalian inner ear (71, 72), and several members of this protein family are connected to genetic causes of HL (73). Further studies on molecular mechanisms will be necessary to evaluate specific contributions of integrins to FRDA-related HL. Finally, in the context of general FRDA pathophysiology and progression, it is important to consider that integrins are transmembrane receptor proteins that are involved in numerous aspects of cell to matrix and cell-to-cell interactions, and their functions are essential for the development and regeneration of central and peripheral nervous systems (48, 49, 74).

Our RPPA screen conducted in primary fibroblast cells identified RA signaling as a pathway affected in FRDA. Expression of the enzymes ALDH1A3 and AOX1, essential for regulation of RA levels, was increased in FRDA cells, resulting in changes in serum ROL concentration in FRDA samples relative to CTRL. Even though patients with FRDA express higher levels of ALDH1A3 and AOX1 proteins than CTRLs, patients with diagnosed CMP express significantly less ALDH1A3 and AOX1 than patients without cardiac symptoms.

expressing FRDA samples (*A*) and CTRL samples. *C*, quantification of ALDH1A3 Western blot from (*B*). A significant difference as calculated by Student's *t* test ($p < 0.05$) is denoted by the *asterisk*. *D*, quantification of FXN Western blot from (*B*). A significant difference as calculated by Student's *t* test ($p < 0.05$) is denoted by the *asterisk*. *E*, XY scatter plot and linear regression analysis of ALDH1A3 expression values as measured by RNA-Seq (*x*-axis) or RPPA (*y*-axis). Results from correlation analyses (Pearson's and Spearman's) are also presented. *F*, gene expression data generated by RNA-Seq analysis of iPSC-differentiated cardiomyocytes derived from an FRDA CMP+ fibroblast line (RPPA ID 58) before and after GAA repeat excision (edited). *G*, retinol concentration (nanomolars) measurements in CTRL (n = 8) and FRDA (n = 10) serum samples. A significant difference as calculated by Student's *t* test is denoted by *asterisks*. *H*, retinol concentration (nanomolars) measurements in FRDA CMP+ (n = 5) and FRDA CMP– (n = 5) samples. A significant difference as calculated by Student's *t* test is denoted by *asterisks*. ALDH1A3, aldehyde dehydrogenase family 1 member A3; CTRL, control; FRDA, Friedreich's ataxia; FXN, frataxin; GAA, guanine–adenine–adenine; iPSC, induced pluripotent stem cell; RPPA, reverse phase protein array.

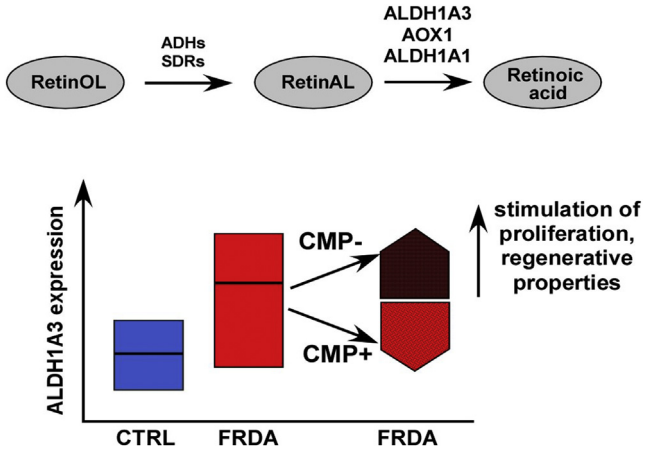

FIG. 7. **Model of ALDH expression and retinol association with FRDA cardiomyopathy.** Expression of several enzymes necessary for biosynthesis of RA is altered in FRDA fibroblasts. ALDH1A3 expression is higher in FRDA samples than in age- and sex-matched controls and is especially increased in FRDA samples derived from individuals without a CMP diagnosis. ALDH, aldehyde dehydrogenase; ALDH1A3, aldehyde dehydrogenase family 1 member A3; CMP, cardiomyopathy; FRDA, Friedreich's ataxia; RA, retinoic acid.

Furthermore, our RNA-Seq results also showed lower levels of *ALDH1A3* mRNA in CMP+ patients (14). Interestingly, one more enzyme involved in retinoid metabolism, ALDH1A1, was significantly decreased ($p = 0.03$) in the CMP+ subpopulation of FRDA samples despite that its expression was not significantly changed between FRDA and CTRL cohorts. Together, these data suggest that retinoid metabolism might be related to the development of cardiac defects in FRDA (Fig. 7).

The mechanistic connection between expression of ALDH enzymes and FRDA, or CMP status in FRDA, is not immediately clear. High expression levels of ALDH1A3 enhance the self-renewal and proliferative potential of human cardiac atrial appendage progenitor cells (75) and mouse neural progenitor cells (76). Results from these studies support the idea that increased expression of ALDH1A3 could be advantageous in terms of proliferation and regenerative capacity of cells in the context of low FXN protein levels (*e.g.*, FRDA cells). Further work will be necessary to define the role of ALDH1A3 expression and activity in FRDA pathophysiology, especially in cell-type specific contexts.

As none of the RA pathway proteins can be readily measured in peripheral tissues, such as blood or plasma, we decided to focus directly on a circulating RA precursor that can be reliably measured, ROL (55, 56). We quantified the levels of ROL in serum samples as a surrogate measure for ALDH1A3/ALDH1A1/AOX1 expression and detected a significant decrease in ROL concentration in FRDA serum samples compared with CTRL, with samples collected from FRDA CMP− patients showing the lowest levels. As ROL is the precursor to RAL, a substrate of ALDH1A1, ALDH1A3, and AOX1, this result is consistent with the observed increased levels of these enzymes in FRDA fibroblast samples (Fig. 7). It is likely that increased levels of these enzymes, catalyzing oxidation of RAL to RA, drives the RA synthesis reaction forward, thereby depleting the pool of circulating ROL. Irrespective of the mechanism responsible for the increased level of serum ROL in FRDA, especially in CMP+ patients, this measurable metabolite could be further evaluated as a prognostic indicator for CMP in FRDA.

FRDA is a progressive, debilitating, and life-shortening condition. Inevitable disease advancement can be monitored by standardized ataxia scales such as FARS/mFARS or International Cooperative Ataxia Rating Scale (77). From a practical drug discovery perspective, relatively slow progression as determined by a change in the FARS/International Cooperative Ataxia Rating Scale score necessitates lengthy clinical trials on relatively large patient cohorts. These conditions are increasingly difficult to meet considering the rare disease status of FRDA and the growing number of clinical trials, underscoring the urgent need for predictive and monitoring biomarker identification. Moreover, another utility of predictive biomarkers is stratification of cohorts for clinical trials, especially if certain interventions are targeting specific symptoms. Therefore, in addition to discovering novel aspects of disease pathogenesis, identifying potential symptom biomarkers and uncovering reliable surrogate end points for clinical trials is of critical importance in FRDA (46). Advances of modern -omics approaches, especially pertaining to quantitative proteomics and metabolomics platforms, are likely to facilitate that process.

DATA AVAILABILITY

Normalized expression data from all samples analyzed on the RPPA are provided in supplemental File S1. Gene expression data from RNA-Seq were published (14) and deposited into the Gene Expression Omnibus database (GSE104288).

Supplemental data—This article contains supplemental data.

Acknowledgments—The authors thank all FRDA and CTRL individuals for their generous donations of skin biopsies for derivation of fibroblast cell lines and serum samples. We thank Kimberly Lin, MD, of CHOP for helpful discussions regarding CMP in patients with FRDA. The authors thank Ms Fuli Jia and Danli Wu, PhD for technical support and the Metabolomics Core at BCM for MS service.

Author contributions—J. S. N., A. C., Y. -Y. C., C. M., P. X., S. H., and M. N. designed and conducted experiments. J. S. N., K. R., C. C., C. M., I. A. B., and M. N. designed data analyses. K. R., C. C., J. S. N., C. M., I. A. B., and M. N. performed data analyses. D. R. L., J. F., and L. A. H. provided FRDA patient skin biopsy material and serum samples. J. S.

N., K. R., C. C., S. H., and M. N. wrote the article. J. S. N., M. N., S. H., D. R. L., and D. P. E. acquired funding. All authors read the article, contributed comments and suggestions, and approved the final version of the article.

Funding and additional information—These studies were supported by research grants from Friedreich's Ataxia Research Alliance and Friedreich's Ataxia Research Alliance Ireland (FARA Ireland) (to M. N. and J. S. N.) and a separate FARA research grant (to D. R. L.). Support was also provided by National Institutes of Health R01NS081366 and R01NS121038 from National Institute of Neurological Disorders and Stroke (to M. N.), the Muscular Dystrophy Association (MDA0789) (to M. N.), and in part by a Cancer Prevention & Research Institute of Texas Proteomics & Metabolomics Core Facility Support Award (RP170005) (to D. P. E. and S. H.), and National Cancer Institute Cancer Center support grant to Antibody-based Proteomics Core/Shared Resource (P30CA125123) (to D. P. E. and S. H.). The content is solely the responsibility of the authors and does not necessarily represent the official views of the National Institutes of Health.

Conflict of interest—The authors declare no competing interests.

Abbreviations—The abbreviations used are: ALDH1A3, aldehyde dehydrogenase family 1 member A3; AOX1, aldehyde oxidase 1; BCM, Baylor College of Medicine; CHOP, Children's Hospital of Philadelphia; CMP, cardiomyopathy; CTRL, control; DE, differentially expressed; FARS, Functional Assessment Rating Scale; FC, fold change; FRDA, Friedreich's ataxia; FXN, frataxin; GAA, guanine–adenine–adenine; H_2O_2, hydrogen peroxide; HL, hearing loss; IRB, Institutional Review Board; ISTD, internal standard; LDH, lactate dehydrogenase; PDT, population doubling time; RA, retinoic acid; RAL, retinal; ROL, retinol; RPPA, reverse phase protein array; UAB, University of Alabama at Birmingham.

Received March 28, 2021 Published, MCPRO Papers in Press, May 13, 2021, https://doi.org/10.1016/j.mcpro.2021.100094

REFERENCES

1. Campuzano, V., Montermini, L., Molto, M. D., Pianese, L., Cossee, M., Cavalcanti, F., Monros, E., Rodius, F., Duclos, F., Monticelli, A., Zara, F., Canizares, J., Koutnikova, H., Bidichandani, S. I., Gellera, C., *et al*. (1996) Friedreich's ataxia: Autosomal recessive disease caused by an intronic GAA triplet repeat expansion. *Science* **271**, 1423–1427
2. Cossee, M., Durr, A., Schmitt, M., Dahl, N., Trouillas, P., Allinson, P., Kostrzewa, M., Nivelon-Chevallier, A., Gustavson, K. H., Kohlschutter, A., Muller, U., Mandel, J. L., Brice, A., Koenig, M., Cavalcanti, F., *et al*. (1999) Friedreich's ataxia: Point mutations and clinical presentation of compound heterozygotes. *Ann. Neurol.* **45**, 200–206
3. Lazaropoulos, M., Dong, Y., Clark, E., Greeley, N. R., Seyer, L. A., Brigatti, K. W., Christie, C., Perlman, S. L., Wilmot, G. R., Gomez, C. M., Mathews, K. D., Yoon, G., Zesiewicz, T., Hoyle, C., Subramony, S. H., *et al*. (2015) Frataxin levels in peripheral tissue in Friedreich ataxia. *Ann. Clin. Transl. Neurol.* **2**, 831–842
4. Deutsch, E. C., Santani, A. B., Perlman, S. L., Farmer, J. M., Stolle, C. A., Marusich, M. F., and Lynch, D. R. (2010) A rapid, noninvasive immunoassay for frataxin: Utility in assessment of Friedreich ataxia. *Mol. Genet. Metab.* **101**, 238–245
5. Delatycki, M. B., and Corben, L. A. (2012) Clinical features of Friedreich ataxia. *J. Child Neurol.* **27**, 1133–1137
6. Parkinson, M. H., Boesch, S., Nachbauer, W., Mariotti, C., and Giunti, P. (2013) Clinical features of Friedreich's ataxia: Classical and atypical phenotypes. *J. Neurochem.* **126 Suppl 1**, 103–117
7. Thoren, C. (1962) Diabetes mellitus in Friedreich's ataxia. *Acta Paediatr.* **135**, 239–247
8. Harding, A. E. (1993) Clinical features and classification of inherited ataxias. *Adv. Neurol.* **61**, 1–14
9. Fortuna, F., Barboni, P., Liguori, R., Valentino, M. L., Savini, G., Gellera, C., Mariotti, C., Rizzo, G., Tonon, C., Manners, D., Lodi, R., Sadun, A. A., and Carelli, V. (2009) Visual system involvement in patients with Friedreich's ataxia. *Brain* **132**, 116–123
10. Rance, G., Corben, L., Barker, E., Carew, P., Chisari, D., Rogers, M., Dowell, R., Jamaluddin, S., Bryson, R., and Delatycki, M. B. (2010) Auditory perception in individuals with Friedreich's ataxia. *Audiol. Neurootol.* **15**, 229–240
11. Coppola, G., Burnett, R., Perlman, S., Versano, R., Gao, F., Plasterer, H., Rai, M., Sacca, F., Filla, A., Lynch, D. R., Rusche, J. R., Gottesfeld, J. M., Pandolfo, M., and Geschwind, D. H. (2011) A gene expression phenotype in lymphocytes from Friedreich ataxia patients. *Ann. Neurol.* **70**, 790–804
12. Nachun, D., Gao, F., Isaacs, C., Strawser, C., Yang, Z., Dokuru, D., Van Berlo, V., Sears, R., Farmer, J., Perlman, S., Lynch, D. R., and Coppola, G. (2018) Peripheral blood gene expression reveals an inflammatory transcriptomic signature in Friedreich's ataxia patients. *Hum. Mol. Genet.* **27**, 2965–2977
13. Haugen, A. C., Di Prospero, N. A., Parker, J. S., Fannin, R. D., Chou, J., Meyer, J. N., Halweg, C., Collins, J. B., Durr, A., Fischbeck, K., and Van Houten, B. (2010) Altered gene expression and DNA damage in peripheral blood cells from Friedreich's ataxia patients: Cellular model of pathology. *PLoS Genet.* **6**, e1000812
14. Napierala, J. S., Li, Y., Lu, Y., Lin, K., Hauser, L. A., Lynch, D. R., and Napierala, M. (2017) Comprehensive analysis of gene expression patterns in Friedreich's ataxia fibroblasts by RNA sequencing reveals altered levels of protein synthesis factors and solute carriers. *Dis. Model. Mech.* **10**, 1353–1369
15. Selak, M. A., Lyver, E., Micklow, E., Deutsch, E. C., Onder, O., Selamoglu, N., Yager, C., Knight, S., Carroll, M., Daldal, F., Dancis, A., Lynch, D. R., and Sarry, J. E. (2011) Blood cells from Friedreich ataxia patients harbor frataxin deficiency without a loss of mitochondrial function. *Mitochondrion* **11**, 342–350
16. Shan, B., Xu, C., Zhang, Y., Xu, T., Gottesfeld, J. M., and Yates, J. R., 3rd (2014) Quantitative proteomic analysis identifies targets and pathways of a 2-aminobenzamide HDAC inhibitor in Friedreich's ataxia patient iPSC-derived neural stem cells. *J. Proteome Res.* **13**, 4558–4566
17. Telot, L., Rousseau, E., Lesuisse, E., Garcia, C., Morlet, B., Leger, T., Camadro, J. M., and Serre, V. (2018) Quantitative proteomics in Friedreich's ataxia B-lymphocytes: A valuable approach to decipher the biochemical events responsible for pathogenesis. *Biochim. Biophys. Acta Mol. Basis Dis.* **1864**, 997–1009
18. Pathak, D., Srivastava, A. K., Padma, M. V., Gulati, S., and Rajeswari, M. R. (2019) Quantitative proteomic and network analysis of differentially expressed proteins in PBMC of Friedreich's ataxia (FRDA) patients. *Front. Neurosci.* **13**, 1054
19. Akbani, R., Becker, K. F., Carragher, N., Goldstein, T., de Koning, L., Korf, U., Liotta, L., Mills, G. B., Nishizuka, S. S., Pawlak, M., Petricoin, E. F., 3rd, Pollard, H. B., Serrels, B., and Zhu, J. (2014) Realizing the promise of reverse phase protein arrays for clinical, translational, and basic research: A workshop report: The RPPA (Reverse Phase Protein Array) society. *Mol. Cell. Proteomics* **13**, 1625–1643
20. Creighton, C. J., and Huang, S. (2015) Reverse phase protein arrays in signaling pathways: A data integration perspective. *Drug Des. Dev. Ther.* **9**, 3519–3527
21. Lu, Y., Ling, S., Hegde, A. M., Byers, L. A., Coombes, K., Mills, G. B., and Akbani, R. (2016) Using reverse-phase protein arrays as pharmacodynamic assays for functional proteomics, biomarker discovery, and drug development in cancer. *Semin. Oncol.* **43**, 476–483
22. Grote, T., Siwak, D. R., Fritsche, H. A., Joy, C., Mills, G. B., Simeone, D., Whitcomb, D. C., and Logsdon, C. D. (2008) Validation of reverse phase

protein array for practical screening of potential biomarkers in serum and plasma: Accurate detection of CA19-9 levels in pancreatic cancer. *Proteomics* **8**, 3051–3060
23. Kuang, Z., Huang, R., Yang, Z., Lv, Z., Chen, X., Xu, F., Yi, Y. H., Wu, J., and Huang, R. P. (2018) Quantitative screening of serum protein biomarkers by reverse phase protein arrays. *Oncotarget* **9**, 32624–32641
24. Morriss, G. R., Rajapakshe, K., Huang, S., Coarfa, C., and Cooper, T. A. (2018) Mechanisms of skeletal muscle wasting in a mouse model for myotonic dystrophy type 1. *Hum. Mol. Genet.* **27**, 2789–2804
25. Li, Y., Polak, U., Clark, A. D., Bhalla, A. D., Chen, Y. Y., Li, J., Farmer, J., Seyer, L., Lynch, D., Butler, J. S., and Napierala, M. (2016) Establishment and maintenance of primary fibroblast repositories for rare diseases-Friedreich's ataxia example. *Biopreserv. Biobank.* **14**, 324–329
26. Li, Y., Lu, Y., Polak, U., Lin, K., Shen, J., Farmer, J., Seyer, L., Bhalla, A. D., Rozwadowska, N., Lynch, D. R., Butler, J. S., and Napierala, M. (2015) Expanded GAA repeats impede transcription elongation through the FXN gene and induce transcriptional silencing that is restricted to the FXN locus. *Hum. Mol. Genet.* **24**, 6932–6943
27. Guo, L., Wang, Q., Weng, L., Hauser, L. A., Strawser, C. J., Rocha, A. G., Dancis, A., Mesaros, C., Lynch, D. R., and Blair, I. A. (2018) Liquid chromatography-high resolution mass spectrometry analysis of platelet frataxin as a protein biomarker for the rare disease Friedreich's ataxia. *Anal. Chem.* **90**, 2216–2223
28. Clay, A., Obrochta, K. M., Soon, R. K., Jr., Russell, C. B., and Lynch, D. R. (2020) Neurofilament light chain as a potential biomarker of disease status in Friedreich ataxia. *J. Neurol.* **267**, 2594–2598
29. Chang, C. H., Zhang, M., Rajapakshe, K., Coarfa, C., Edwards, D., Huang, S., and Rosen, J. M. (2015) Mammary stem cells and tumor-initiating cells are more resistant to apoptosis and exhibit increased DNA repair activity in response to DNA damage. *Stem Cell Rep.* **5**, 378–391
30. Bu, W., Liu, Z., Jiang, W., Nagi, C., Huang, S., Edwards, D. P., Jo, E., Mo, Q., Creighton, C. J., Hilsenbeck, S. G., Leavitt, A. D., Lewis, M. T., Wong, S. T. C., and Li, Y. (2019) Mammary precancerous stem and non-stem cells evolve into cancers of distinct subtypes. *Cancer Res.* **79**, 61–71
31. Coarfa, C., Grimm, S. L., Rajapakshe, K., Perera, D., Lu, H. Y., Wang, X., Christensen, K. R., Mo, Q., Edwards, D. P., and Huang, S. (2021) Reverse-phase protein array: Technology, application, data processing, and integration. *J. Biomol. Tech.* https://doi.org/10.7171/jbt.2021-3202-001
32. Bradford, M. M. (1976) A rapid and sensitive method for the quantitation of microgram quantities of protein utilizing the principle of protein-dye binding. *Anal. Biochem.* **72**, 248–254
33. Amara, C. S., Ambati, C. R., Vantaku, V., Badrajee Piyarathna, D. W., Donepudi, S. R., Ravi, S. S., Arnold, J. M., Putluri, V., Chatta, G., Guru, K. A., Badr, H., Terris, M. K., Bollag, R. J., Sreekumar, A., Apolo, A. B., *et al*. (2019) Serum metabolic profiling identified a distinct metabolic signature in bladder cancer smokers: A key metabolic enzyme associated with patient survival. *Cancer Epidemiol. Biomarkers Prev.* **28**, 770–781
34. Vantaku, V., Donepudi, S. R., Piyarathna, D. W. B., Amara, C. S., Ambati, C. R., Tang, W., Putluri, V., Chandrashekar, D. S., Varambally, S., Terris, M. K., Davies, K., Ambs, S., Bollag, R., Apolo, A. B., Sreekumar, A., *et al*. (2019) Large-scale profiling of serum metabolites in African American and European American patients with bladder cancer reveals metabolic pathways associated with patient survival. *Cancer* **125**, 921–932
35. Jiang, L., Luo, M., Liu, D., Chen, B., Zhang, W., Mai, L., Zeng, J., Huang, N., Huang, Y., Mo, X., and Li, W. (2013) BAD overexpression inhibits cell growth and induces apoptosis via mitochondrial-dependent pathway in non-small cell lung cancer. *Cancer Cell Int.* **13**, 53
36. Green, D. R., and Llambi, F. (2015) Cell death signaling. *Cold Spring Harb. Perspect. Biol.* **7**, a006080
37. Yue, J., and Lopez, J. M. (2020) Understanding MAPK signaling pathways in apoptosis. *Int. J. Mol. Sci.* **21**, 2346
38. Shi, Y. (2002) Mechanisms of caspase activation and inhibition during apoptosis. *Mol. Cell* **9**, 459–470
39. Wong, A., Yang, J., Cavadini, P., Gellera, C., Lonnerdal, B., Taroni, F., and Cortopassi, G. (1999) The Friedreich's ataxia mutation confers cellular sensitivity to oxidant stress which is rescued by chelators of iron and calcium and inhibitors of apoptosis. *Hum. Mol. Genet.* **8**, 425–430
40. Abeti, R., Baccaro, A., Esteras, N., and Giunti, P. (2018) Novel Nrf2-inducer prevents mitochondrial defects and oxidative stress in Friedreich's ataxia models. *Front. Cell. Neurosci.* **12**, 188
41. Chen, G., Luo, Y., Warncke, K., Sun, Y., Yu, D. S., Fu, H., Behera, M., Ramalingam, S. S., Doetsch, P. W., Duong, D. M., Lammers, M., Curran, W. J., and Deng, X. (2019) Acetylation regulates ribonucleotide reductase activity and cancer cell growth. *Nat. Commun.* **10**, 3213
42. Yang, C., Sengupta, S., Hegde, P. M., Mitra, J., Jiang, S., Holey, B., Sarker, A. H., Tsai, M. S., Hegde, M. L., and Mitra, S. (2017) Regulation of oxidized base damage repair by chromatin assembly factor 1 subunit A. *Nucleic Acids Res.* **45**, 739–748
43. Vire, E., Brenner, C., Deplus, R., Blanchon, L., Fraga, M., Didelot, C., Morey, L., Van Eynde, A., Bernard, D., Vanderwinden, J. M., Bollen, M., Esteller, M., Di Croce, L., de Launoit, Y., and Fuks, F. (2006) The polycomb group protein EZH2 directly controls DNA methylation. *Nature* **439**, 871–874
44. Morisaki, H., Fujimoto, A., Ando, A., Nagata, Y., Ikeda, K., and Nakanishi, M. (1997) Cell cycle-dependent phosphorylation of p27 cyclin-dependent kinase (Cdk) inhibitor by cyclin E/Cdk2. *Biochem. Biophys. Res. Commun.* **240**, 386–390
45. Vlach, J., Hennecke, S., and Amati, B. (1997) Phosphorylation-dependent degradation of the cyclin-dependent kinase inhibitor p27. *EMBO J.* **16**, 5334–5344
46. Blair, I. A., Farmer, J., Hersch, S., Larkindale, J., Lynch, D. R., Napierala, J., Napierala, M., Payne, R. M., and Subramony, S. H. (2019) The current state of biomarker research for Friedreich's ataxia: A report from the 2018 FARA biomarker meeting. *Future Sci. OA* **5**, FSO398
47. Pytela, R., Pierschbacher, M. D., and Ruoslahti, E. (1985) Identification and isolation of a 140 kd cell surface glycoprotein with properties expected of a fibronectin receptor. *Cell* **40**, 191–198
48. Lefcort, F., Venstrom, K., McDonald, J. A., and Reichardt, L. F. (1992) Regulation of expression of fibronectin and its receptor, alpha 5 beta 1, during development and regeneration of peripheral nerve. *Development* **116**, 767–782
49. Lilja, J., and Ivaska, J. (2018) Integrin activity in neuronal connectivity. *J. Cell Sci.* **131**, jcs212803
50. Payne, R. M., and Wagner, G. R. (2012) Cardiomyopathy in Friedreich ataxia: Clinical findings and research. *J. Child Neurol.* **27**, 1179–1186
51. Lu, C., Schoenfeld, R., Shan, Y., Tsai, H. J., Hammock, B., and Cortopassi, G. (2009) Frataxin deficiency induces Schwann cell inflammation and death. *Biochim. Biophys. Acta* **1792**, 1052–1061
52. Li, J., Rozwadowska, N., Clark, A., Fil, D., Napierala, J. S., and Napierala, M. (2019) Excision of the expanded GAA repeats corrects cardiomyopathy phenotypes of iPSC-derived Friedreich's ataxia cardiomyocytes. *Stem Cell Res.* **40**, 101529
53. Mic, F. A., Molotkov, A., Fan, X., Cuenca, A. E., and Duester, G. (2000) RALDH3, a retinaldehyde dehydrogenase that generates retinoic acid, is expressed in the ventral retina, otic vesicle and olfactory pit during mouse development. *Mech. Dev.* **97**, 227–230
54. Belyaeva, O. V., Adams, M. K., Popov, K. M., and Kedishvili, N. Y. (2019) Generation of retinaldehyde for retinoic acid biosynthesis. *Biomolecules* **10**, 5
55. Molina, J. A., de Bustos, F., Jimenez-Jimenez, F. J., Esteban, J., Guerrero-Sola, A., Zurdo, M., Orti-Pareja, M., Gasalla, T., Gomez-Escalonilla, C., Ramirez-Ramos, C., Guillamon, F., and Arenas, J. (1999) Serum levels of beta-carotene, alpha-carotene, and vitamin A in patients with amyotrophic lateral sclerosis. *Acta Neurol. Scand.* **99**, 315–317
56. da Silva, R., dos Santos-Valente, E. C., Burim Scomparini, F., Saccardo Sarni, R. O., and Costa-Carvalho, B. T. (2014) The relationship between nutritional status, vitamin A and zinc levels and oxidative stress in patients with ataxia-telangiectasia. *Allergol. Immunopathol. (Madr.)* **42**, 329–335
57. Palomo, G. M., Cerrato, T., Gargini, R., and Diaz-Nido, J. (2011) Silencing of frataxin gene expression triggers p53-dependent apoptosis in human neuron-like cells. *Hum. Mol. Genet.* **20**, 2807–2822
58. Mincheva-Tasheva, S., Obis, E., Tamarit, J., and Ros, J. (2014) Apoptotic cell death and altered calcium homeostasis caused by frataxin depletion in dorsal root ganglia neurons can be prevented by BH4 domain of Bcl-xL protein. *Hum. Mol. Genet.* **23**, 1829–1841
59. Loria, F., and Diaz-Nido, J. (2015) Frataxin knockdown in human astrocytes triggers cell death and the release of factors that cause neuronal toxicity. *Neurobiol. Dis.* **76**, 1–12
60. Herman, D., Jenssen, K., Burnett, R., Soragni, E., Perlman, S. L., and Gottesfeld, J. M. (2006) Histone deacetylase inhibitors reverse gene silencing in Friedreich's ataxia. *Nat. Chem. Biol.* **2**, 551–558

61. Greene, E., Mahishi, L., Entezam, A., Kumari, D., and Usdin, K. (2007) Repeat-induced epigenetic changes in intron 1 of the frataxin gene and its consequences in Friedreich ataxia. *Nucleic Acids Res.* **35**, 3383–3390
62. Punga, T., and Buhler, M. (2010) Long intronic GAA repeats causing Friedreich ataxia impede transcription elongation. *EMBO Mol. Med.* **2**, 120–129
63. Kim, E., Napierala, M., and Dent, S. Y. (2011) Hyperexpansion of GAA repeats affects post-initiation steps of FXN transcription in Friedreich's ataxia. *Nucleic Acids Res.* **39**, 8366–8377
64. Chan, P. K., Torres, R., Yandim, C., Law, P. P., Khadayate, S., Mauri, M., Grosan, C., Chapman-Rothe, N., Giunti, P., Pook, M., and Festenstein, R. (2013) Heterochromatinization induced by GAA-repeat hyperexpansion in Friedreich's ataxia can be reduced upon HDAC inhibition by vitamin B3. *Hum. Mol. Genet.* **22**, 2662–2675
65. Lai, J. I., Nachun, D., Petrosyan, L., Throesch, B., Campau, E., Gao, F., Baldwin, K. K., Coppola, G., Gottesfeld, J. M., and Soragni, E. (2019) Transcriptional profiling of isogenic Friedreich ataxia neurons and effect of an HDAC inhibitor on disease signatures. *J. Biol. Chem.* **294**, 1846–1859
66. Durr, A., Cossee, M., Agid, Y., Campuzano, V., Mignard, C., Penet, C., Mandel, J. L., Brice, A., and Koenig, M. (1996) Clinical and genetic abnormalities in patients with Friedreich's ataxia. *N. Engl. J. Med.* **335**, 1169–1175
67. Rance, G., Fava, R., Baldock, H., Chong, A., Barker, E., Corben, L., and Delatycki, M. B. (2008) Speech perception ability in individuals with Friedreich ataxia. *Brain* **131**, 2002–2012
68. Giraudet, F., Charles, P., Mom, T., Boespflug-Tanguy, O., Durr, A., Deltenre, P., and Avan, P. (2018) Rapid exhaustion of auditory neural conduction in a prototypical mitochondrial disease, Friedreich ataxia. *Clin. Neurophysiol.* **129**, 1121–1129
69. Maudoux, A., Teissier, N., Francois, M., Van Den Abbeele, T., Alberti, C., Husson, I., and Wiener-Vacher, S. R. (2020) Vestibular impact of Friedreich ataxia in early onset patients. *Cerebellum Ataxias* **7**, 6
70. Brunetta, I., Casalotti, S. O., Hart, I. R., Forge, A., and Reynolds, L. E. (2012) beta3-Integrin is required for differentiation in OC-2 cells derived from mammalian embryonic inner ear. *BMC Cell Biol.* **13**, 5
71. Littlewood Evans, A., and Muller, U. (2000) Stereocilia defects in the sensory hair cells of the inner ear in mice deficient in integrin alpha8beta1. *Nat. Genet.* **24**, 424–428
72. Davies, D., Magnus, C., and Corwin, J. T. (2007) Developmental changes in cell-extracellular matrix interactions limit proliferation in the mammalian inner ear. *Eur. J. Neurosci.* **25**, 985–998
73. Crompton, M., Purnell, T., Tyrer, H. E., Parker, A., Ball, G., Hardisty-Hughes, R. E., Gale, R., Williams, D., Dean, C. H., Simon, M. M., Mallon, A. M., Wells, S., Bhutta, M. F., Burton, M. J., Tateossian, H., *et al*. (2017) A mutation in Nischarin causes otitis media via LIMK1 and NF-kappaB pathways. *PLoS Genet.* **13**, e1006969
74. Vogelezang, M. G., Liu, Z., Relvas, J. B., Raivich, G., Scherer, S. S., and ffrench-Constant, C. (2001) Alpha4 integrin is expressed during peripheral nerve regeneration and enhances neurite outgrowth. *J. Neurosci.* **21**, 6732–6744
75. Puttini, S., Plaisance, I., Barile, L., Cervio, E., Milano, G., Marcato, P., Pedrazzini, T., and Vassalli, G. (2018) ALDH1A3 is the key isoform that contributes to aldehyde dehydrogenase activity and affects *in vitro* proliferation in cardiac atrial appendage progenitor cells. *Front. Cardiovasc. Med.* **5**, 90
76. La Rosa, P., Bielli, P., Compagnucci, C., Cesari, E., Volpe, E., Farioli Vecchioli, S., and Sette, C. (2016) Sam68 promotes self-renewal and glycolytic metabolism in mouse neural progenitor cells by modulating Aldh1a3 pre-mRNA 3'-end processing. *Elife* **5**, e20750
77. Burk, K., Schulz, S. R., and Schulz, J. B. (2013) Monitoring progression in Friedreich ataxia (FRDA): The use of clinical scales. *J. Neurochem.* **126 Suppl 1**, 118–124